(4)

AD-A228 359

CPS SUPERCONDUCTOR
CORPORATION

NINTH QUARTERLY REPORT

FOR THE PROJECT

"COMPOSITE CERAMIC SUPERCONDUCTING WIRES FOR ELECTRIC MOTOR APPLICATIONS"

PRIME CONTRACTOR

CPS SUPERCONDUCTOR CORPORATION
A Subsidiary of
Ceramics Process Systems Corporation
155 Fortune Boulevard
Milford, Massachusetts 01757

September 30, 1990

DARPA Order Number: 9525
Contract Number: N00014-88-C-0512
Contract Effective Date: June 30, 1988
Contract Expiration Date: March 31, 1991
Principal Investigator: James D. Hodge
(508) 634-3422

Prepared for:

Defense Advanced Research Projects Agency
1400 Wilson Boulevard
Arlington, VA 22209

Office of Naval Research
800 North Quincy Street
Arlington, VA 22217

REPORT DOCUMENTATION PAGE

Form Approved
OMB No. 0704-0188

1. AGENCY USE ONLY (Leave blank)	2. REPORT DATE	3. REPORT TYPE AND DATES COVERED
	9/30/90	7/1/90 - 9/30/90

4. TITLE AND SUBTITLE
Composite Ceramic Superconducting Wires for Electric Motor Applications

5. FUNDING NUMBERS
N00014-88-C-0512

6. AUTHOR(S)
Dr. James D. Hodge

7. PERFORMING ORGANIZATION NAME(S) AND ADDRESS(ES)
CPS Superconductor Corporation
155 Fortune Blvd.
Milford, MA 01757

8. PERFORMING ORGANIZATION REPORT NUMBER
CPSS-0990-1

9. SPONSORING/MONITORING AGENCY NAME(S) AND ADDRESS(ES)
Defense Advanced Research Projects Agency
1400 Wilson Boulevard, Arlington, VA 22209

Office of Naval Research
800 North Quincy Street, Arlington, VA 22217-500

10. SPONSORING/MONITORING AGENCY REPORT NUMBER

11. SUPPLEMENTARY NOTES
N/A

12a. DISTRIBUTION/AVAILABILITY STATEMENT
Unlimited

12b. DISTRIBUTION CODE

13. ABSTRACT (Maximum 200 words)

A scaled-up process for producing sintered, silver-coated YBCO monofilament wire has been developed and is currently able to produce 30 meters of wire/day. Efforts aimed at improving the electrical performance of this wire are well underway. Two approaches are being used: 1) Continuously melt-texturing sintered YBCO wire/fiber to produce a macro-crystalline, strong-linked wire, and 2) Adapt the YBCO process to the production of BiSCCO wire which can be subsequently mechanically textured by rolling the wire into ribbon.

Work has also proceeded on the fabrication of a brushless DC "trapped flux" motor in which melt-textured YBCO rings are used as permanent magnet "replicas". This motor design holds the potential for a high power density HTSC motor which can be fabricated using current HTSC technology.

14. SUBJECT TERMS	15. NUMBER OF PAGES
Superconductor, ceramic, motor	50
	16. PRICE CODE

17. SECURITY CLASSIFICATION OF REPORT	18. SECURITY CLASSIFICATION OF THIS PAGE	19. SECURITY CLASSIFICATION OF ABSTRACT	20. LIMITATION OF ABSTRACT
Unclassified	Unclassified	Unclassified	

EXECUTIVE SUMMARY

This report describes progress on the development of a process for producing technologically useful HTSC wire and the application of this wire to the fabrication of a prototype HTSC electric motor. In addition to the continued optimization of the continuous sintered wire process developed under this contract, discussed in detail in previous reports, wire development activities in the past quarter have focused primarily on the improvement of the critical current density of wire produced via the this wire process. Two techniques for improving critical currents are being pursued: the continuous production of melt-textured YBCO fiber/wire, and the adaptation of the wire process to the production of sintered BiSCCO wire which can be subsequently be mechanically textured to yield high J_c wire.

Our attempts to melt-texture YBCO fiber and wire produced by our process have been very successful. Fibers have been produced which show a transport J_c of 18,000 A/cm^2 at 1 Tesla and 77 K. These fibers are produced continuously and lengths of up to 1.0 meter have been successfully textured. Work this past quarter has striven to understand the relationship between processing conditions, microstructure, and electrical characteristics. We have also designed, built, and placed into service a second generation melt-texture furnace which will significantly enhance our capabilities in this area.

Our first BiSCCO ribbon wire was produced this past quarter. Preliminary work in this area has been aimed at the development of a robust process for producing a reproducible BiSCCO powder for use as process feedstock. With this powder process essentially being defined this past quarter, efforts at wire production have, consequently, intensified.

The DC homopolar motor designed by Emerson Electric for use as a test bed for the wire produced in this program has been extensively tested this past quarter using copper windings. It is ready for operation with HTSC wire pending availability of acceptable coils. Work has also proceeded on the design and construction of a brushless "trapped flux permanent magnet" motor. This design, essentially a permanent magnet motor where melt-textured YBCO magnet "replicas" are used in place of conventional magnets, has been fabricated and is presently awaiting the production of the YBCO magnet replicas.

TABLE OF CONTENTS

1. PROGRAM SUMMARY 1

2. PROGRAM STATUS 1
- 2.1 Raw Materials Synthesis and Production 6
  - 2.1.1. Off-Stoichiometric and Substituted $YBa_2Cu_3O_{7-x}$ 6
  - 2.1.2. $Bi_2Ca_2Sr_2Cu_3O_{10}$ Powder Synthesis 7
  - 2.1.3. $YBa_2Cu_3O_{7-x}$ Powder Synthesis 11
- 2.2. Fiber Spinning 14
  - 2.2.1. Melt Spinning of Superconducting Ceramic Fibers 14
  - 2.2.2. Winder Design 15
- 2.3. Wire and Part Development 16
  - 2.3.1. YBCO Sintered Wire 17
  - 2.3.2. Melt-Textured YBCO Fibers 19
  - 2.3.3. Melt-Textured YBCO Pellets 24
  - 2.3.4. BiSCCO Wire Development 29
- 2.4. Motor Design and Fabrication 32
  - 2.4.1. Iron Core Homopolar Motor 33
  - 2.4.2. Brushless DC "Trapped Flux" HTSC Motor 40
  - 2.4.3. Motor Activity Summary 45

3. GOALS FOR FUTURE REPORTING PERIOD 48

4. FINANCIAL STATUS 50

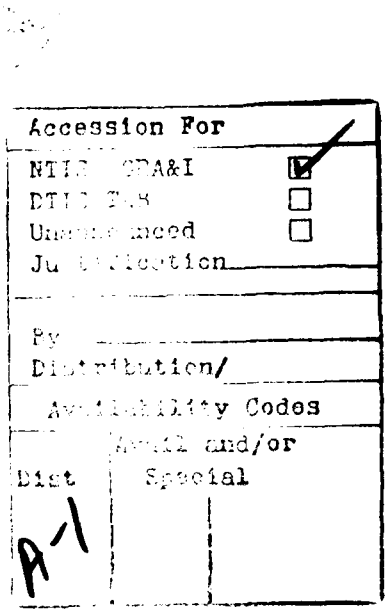

LIST OF FIGURES

Figure 2.1 Revised Project Schedule for Fiber 3
Figure 2.2 Revised Project Schedule for Wire Tasks. 4
Figure 2.3 Project Schedule for HTSC Motor Task 5
Figure 2.4 SEM micrograph of CPS Superconductor BiSCCO powder. 9
Figure 2.5 XRD pattern of BiSCCO powder calcined at 830°C for 30 hours. 10
Figure 2.6 A.C. susceptibility trace of BiSCCO powder calcined at 830°C, 30 hours. 10
Figure 2.7 X-ray diffraction pattern of YBCO calcined prior to recent process changes. 13
Figure 2.8 X-ray diffraction pattern of YBCO calcined with low temperature dwell and reduced CO_2 pressure. 13
Figure 2.9 Section of wind-and-fire coil produced at CPS Superconductor as a HF antenna component. 18
Figure 2.10 J_c plot for wind-and-fire coil, 9 cm long containing 170 cm of fiber. 18
Figure 2.11 Longitudinal section of fiber textured at 4.2 mm/hr. 20
Figure 2.12 Longitudinal section of fiber textured at 12.6 mm/hr. 20
Figure 2.13 Critical current versus magnetic field data for a variety of melt-textured fibers. 22
Figure 2.14 Second phase present between impinged YBCO grains in a phase pure melt-textured pellet. 27
Figure 2.15 Interface between directional crystallization and spherulitic crystallization zones in melt-textured YBCO. 29
Figure 2.16 Presintered Ag-coated BiSCCO Wire. 31
Figure 2.17 Presintered BiSCCO wire after rolling. 31
Figure 2.18 Cross section of the steel core homopolar DC motor with HTSC field windings. 34
Figure 2.19 Flux through field coil versus field coil Ampere turns. 35
Figure 2.20 Back EMF of homopolar DC motor versus field current at 1500 RPM. Designed field current of 0.125 Amperes is marked. 36
Figure 2.21 Voltage drop across brushes and leads versus current in homopolar DC motor in room temperature air. 37
Figure 2.22 No load speed and current versus voltage measured in room temperature air and liquid nitrogen. 39
Figure 2.23 Rotor of the brushless DC trapped flux motor. 41
Figure 2.24 Stator of the brushless DC trapped flux motor. 43
Figure 2.25 The stator is energized while the HTSC rings on rotor are above T_c. 44
Figure 2.26 Currents in the HTSC rings on the rotor maintain the magnetic field after the stator current is turned off. 46

Figure 2.27 Current in the stator windings while the field is trapped in the rotor produces torque. 47

COMPOSITE CERAMIC SUPERCONDUCTING WIRES FOR ELECTRIC MOTOR APPLICATIONS

James D. Hodge
Principal Investigator
CPS Superconductor Corporation
Milford, MA 01757

1. PROGRAM SUMMARY

This Ninth Quarterly Report covers activities during July through September 1990 on a program aimed at the development of high temperature superconducting (HTSC) wire and the utilization of this wire in a prototype superconducting motor. At present the program is being carried out by CPS Superconductor Corporation, a subsidiary of Ceramics Process Systems Corporation, who has the responsibility for wire and materials development, and two subcontractors: Albany International Research Corporation (AIResCo), who has the responsibility for development and production of green fibers and fiber assemblies, and the Emerson Motor Division (EMD) of Emerson Electric, who has the responsibility for the design and construction of the program's HTSC motor.

2. PROGRAM STATUS

This past quarter has marked a change in the program emphasis from the production of quantities of sintered wire to the implementation of processes to improve the electrical behavior this wire. In this regard, efforts in the areas of melt-texturing of $YBa_2Cu_3O_{7-x}$ fibers and wires and mechanical texturing of $Bi_2Ca_2Sr_2Cu_3O_{10}$ wires have been intensified and substantial progress has been made.

In addition, the effort at EMD has shifted from the DC homopolar motor design, which would have required substantial quantities of HTSC wire with performance characteristics presently unavailable, to the "trapped-flux" motor design which can be executed using HTSC materials presently available.

The status of the program is compared with individual tasks of the revised Statement of Work in Figure 1.31, Figure 2.1, Figure 2.1, Figure 2.2, and Figure 2.2, Figure 2.3, which show timelines for the major fiber and wire development tasks. The fiber spinning tasks, as shown, involve both $YBa_2Cu_3O_{7-x}$ and $Bi_2Ca_2Sr_2Cu_3O_{10}$ melt spinning and braiding. These tasks will be extended through 1990. The wire tasks show several of the changes as the program has evolved. The main effort now involves silver coated and co-fired monofilament wire, with braided multifilamentary wire as a secondary effort. The newer activities involving melt texturing $YBa_2Cu_3O_{7-x}$ fiber/wire and mechanically textured $Bi_2Ca_2Sr_2Cu_3O_{10}$, now appear in the list of tasks. We are no longer working on multifilament ribbon wire, as it was originally envisioned, as this has been supplanted by work on braids. The HTSC motor tasks are on schedule, but do not involve testing with HTSC coils, since we have not yet produced complete coils. In addition, the emphasis within the motor task has shifted to the production of a "trapped-flux" machine as this design is within the capabilities of present HTSC technology.

The following sections describe in detail the progress within the program. Section 2.1 covers efforts in raw material (powder) synthesis and production conducted at CPS Superconductor. Section 2.2 details the fiber spinning work

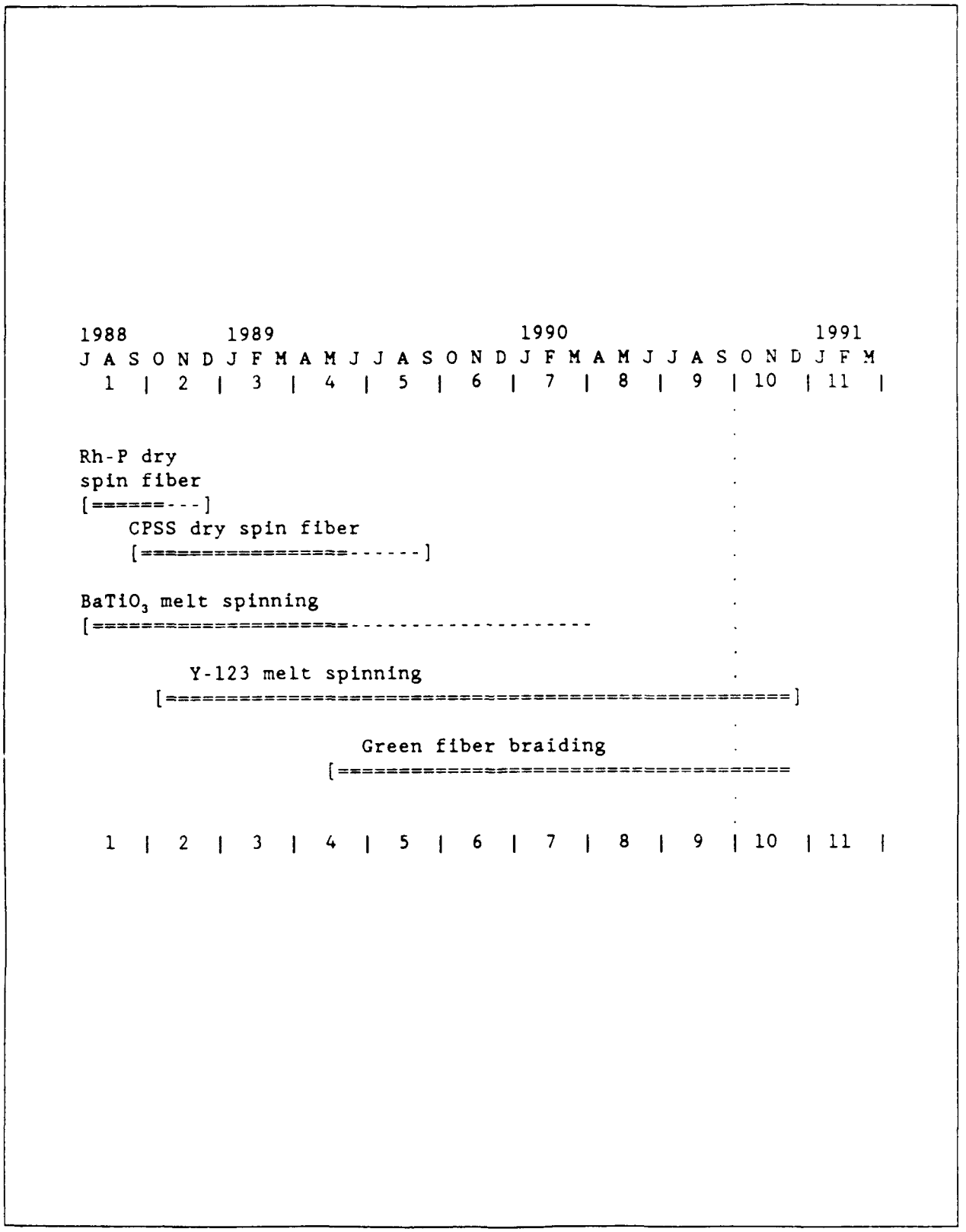

Figure 2.1 Revised Project Schedule for Fiber

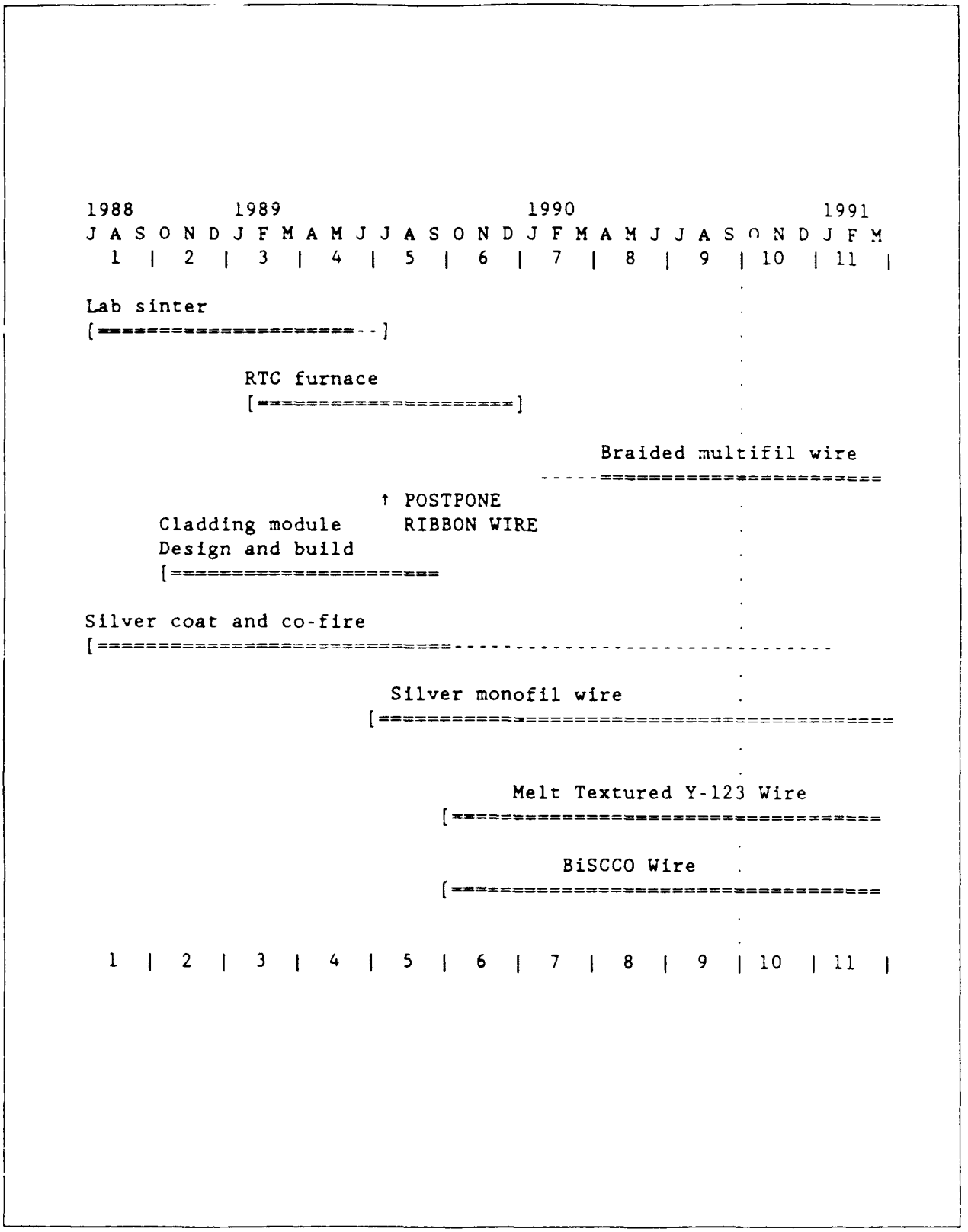

Figure 2.2 Revised Project Schedule for Wire Tasks.

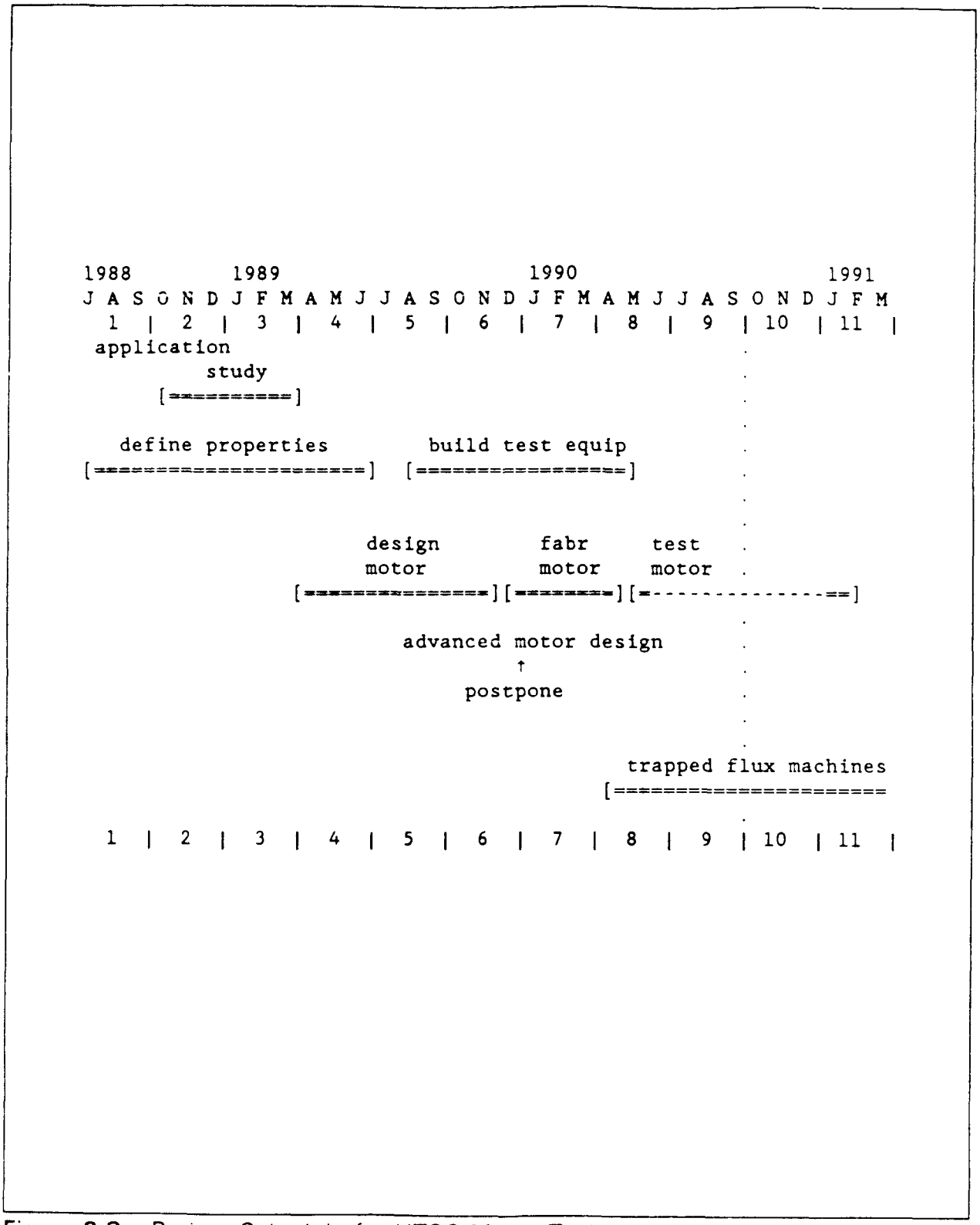

Figure 2.3 Project Schedule for HTSC Motor Task

conducted at Albany International Research Corporation in Mansfield, Massachusetts. Section 2.3 describes wire and fiber cladding, sintering/thermal processing, and characterization work conducted at CPS Superconductor. Section 2.4 outlines the HTSC motor design activities at Emerson Motor Division.

2.1 Raw Materials Synthesis and Production

L.J. Klemptner, Hyun D. Park, and D. Gobielle
CPS Superconductor Corporation

This past quarter has seen an increase in activities in this area as materials development work has been accelerated. Greater effort has been placed on the synthesis of off-stoichiometric and rare earth-substituted YBCO compositions and BiSCCO materials. In addition, an increased understanding of the reactions taking place during the formation of YBCO at high temperatures has enabled us to substantially improve the phase purity of our YBCO powder.

2.1.1. Off-Stoichiometric and Substituted $YBa_2Cu_3O_{7-x}$

While previous work within the program has focussed almost exclusively on phase pure YBCO, our work on melt-texturing has introduced the need for a wider variety of YBCO-based compositions. Specifically, in this past quarter, we have produced mixtures of YBCO and Y_2BaCuO_5 (211) and the rare-earth substituted NdBCO and GdBCO compounds in support of our melt-texturing efforts. All of these compounds have been produced for use in fiber spinning which has necessitated their production in kilogram quantities.

Mixtures of 211 and YBCO were produced by blending appropriate amounts of the prereacted components. This route was chosen to allow a better control of the phases present in the mixture. Experience has shown that attempting to react such an off-stoichiometric mixture in-situ would result in the formation unwanted tertiary phases as the excess Y_2O_3 present in the starting mixture would alter the reaction path during YBCO and 211 formation. The 211 required for these mixtures was made in-house using a modification of the proprietary CPS Superconductor YBCO synthesis method which starts with a mixture of oxides and carbonates and, through a careful control of reactant distribution, reaction atmosphere, and thermal cycle, forms a highly phase-pure final powder. Mixtures of YBCO and 211 were made by vibro-milling appropriate amounts of these compounds overnight in cyclohexane with a dispersant added using zirconia media. Upon drying, these powder mixtures are ready for fiber spinning.

Rare-earth substituted 123 compounds are also being produced for the CPS Superconductor melt-texturing studies. The production of these compounds involves the straightforward substitution of the appropriate rare earth oxide for Y_2O_3 as the starting material in the CPS Superconductor powder process. To date, gadolinium- and neodynium-substituted compounds have been attempted, but have not yet been made into fibers.

2.1.2. $Bi_2Ca_2Sr_2Cu_3O_{10}$ Powder Synthesis

The development of a process for producing BiSCCO powder at CPS Superconductor was initiated under the same guidelines as were used to develop the

YBCO process two years ago, i.e., use of inexpensive, easy to handle raw materials and capability for economical scale-up to kilogram levels of production. As before, a process utilizing a precursor made up of mechanically mixed oxide and carbonate raw materials was selected. Based on a review of the literature, a lead-doped 2223 BiSCCO composition was selected as a starting point for this work. The development work has investigated three fundamental variables: stoichiometry (a variety of Pb/Bi ratios were investigated, as well as excess Ca and Cu and a number of minor dopants), calcining atmosphere, and calcination time and temperature. The goal in optimizing each of these variables was to maximize the amount of the 2223 phase present in as short a calcination time as possible. This work was detailed in the last quarterly report.

This initial screening of these variables produced two viable compositions, BP5 ($Bi_{1.2}Pb_{0.8}Ca_2Sr_2Cu_3O_{10}$) and BPH2 ($Bi_{1.7}Pb_{0.3}Ca_2Sr_2Cu_3O_{10}$) with attendant calcination conditions for scale-up. Scale-up is presently being accomplished through a straightforward modification of the process presently used to manufacture YBCO powder. Further work using the scaled-up processing of these compositions is enabling us to refine our processing conditions to produce material with an even high fraction of 2223. As reported last quarter, precursor powders are initially calcined at 775°C for 6 hours. This is followed by extended heating at 830°C for periods between 30 and 120 hours. While initial calcination studies were performed in air, improvements in powder phase purity have resulted by diluting ambient air with nitrogen. As in the case of YBCO, a key to process scale-up is insuring that the

entire powder bed has access to the flowing ambient gas. This allows decomposition products, i.e., CO_2, to be quickly swept away from the reacting mass and also insures that the entire bed sees a uniform oxygen partial pressure. The formation of 2223 at 830°C is initially very rapid. After 30 hours, approximately the material is approximately 90% 2223. Subsequently, however, this reaction slows considerably, reaching 95% 2223 after a 90 hour calcination. Figure 2.4 shows a representative morphology of the powder produced using this process. Figure 2.5 and Figure 2.6 show a representative x-ray diffraction pattern and A.C. susceptibility trace of CPS Superconductor BiSCCO powder calcined at 830°C for 60 hours.

Figure 2.4 SEM micrograph of CPS Superconductor BiSCCO powder.

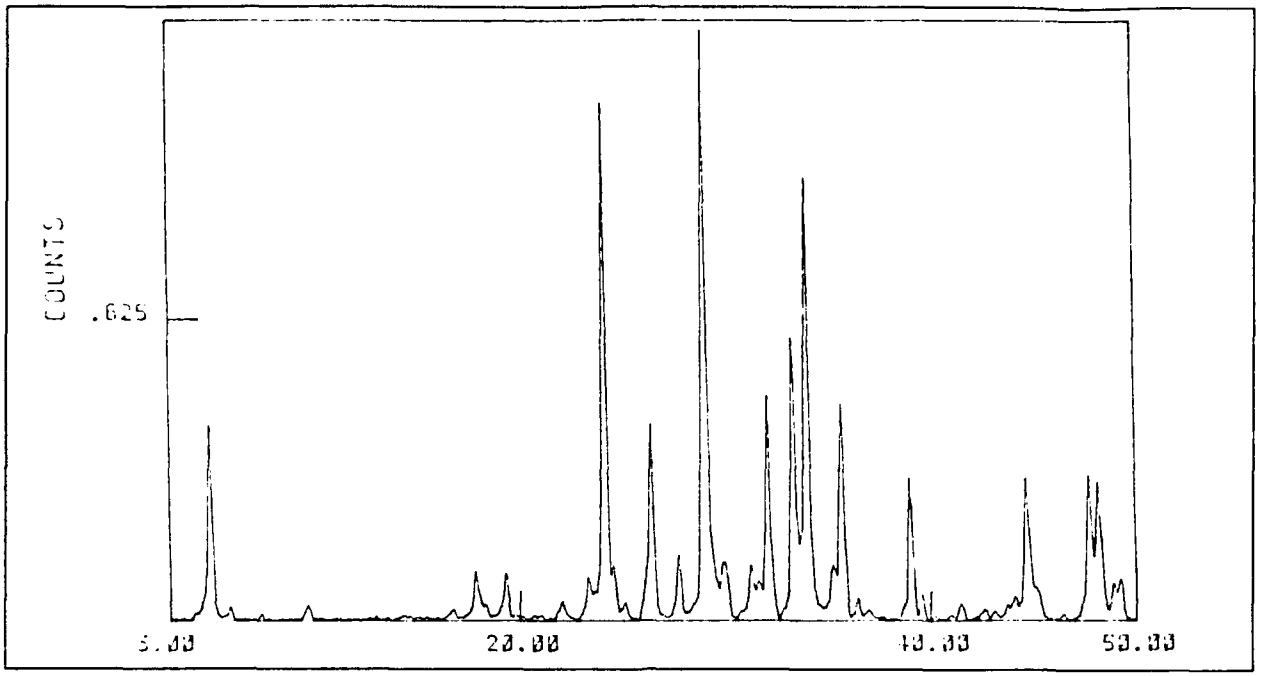

Figure 2.5 XRD pattern of BiSCCO powder calcined at 830°C for 30 hours.

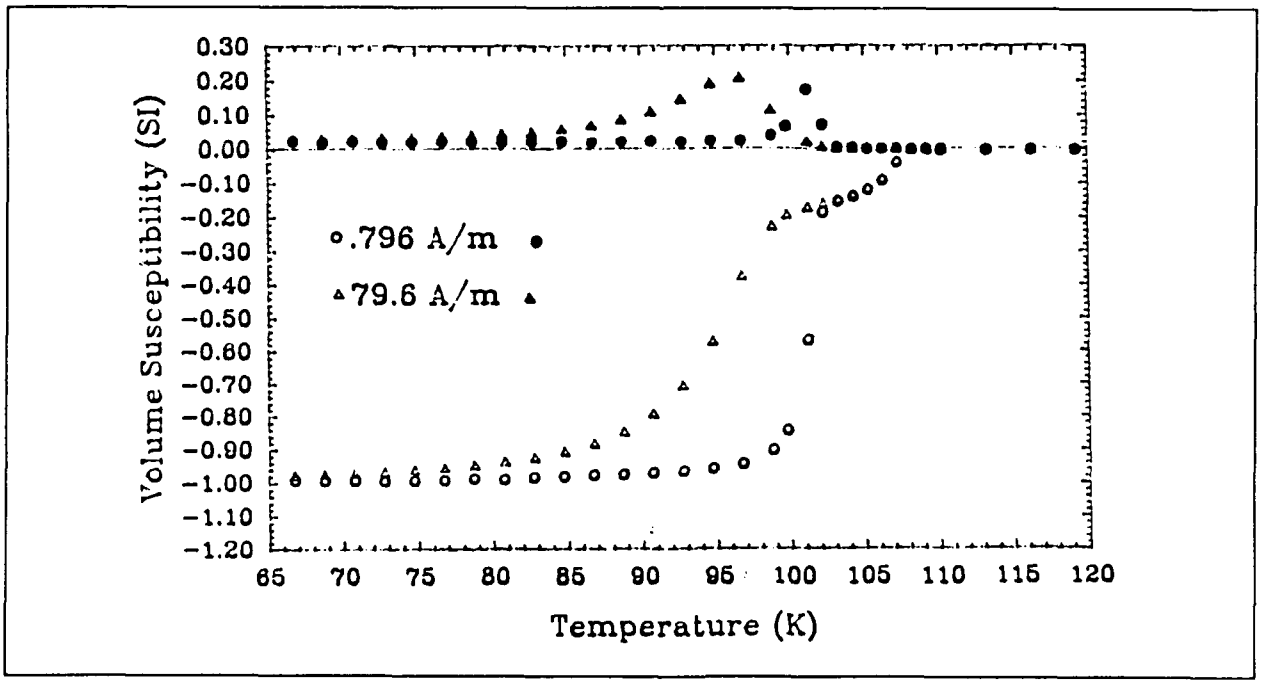

Figure 2.6 A.C. susceptibility trace of BiSCCO powder calcined at 830°C, 30 hours.

2.1.3. $YBa_2Cu_3O_{7-x}$ Powder Synthesis

The bulk of the raw material produced at CPS Superconductor continues to be YBCO and the optimization of the CPS Superconductor powder process is on-going. While the phase and chemical purity of the material produced to date have proven adequate for downstream processing, studies of the reaction between component oxides (and precursor carbonates) to form YBCO carried out over the past year have resulted in the alteration of processing conditions which have reduced secondary phases and residual carbon substantially. These studies investigated both the effects of temperature and starting materials on the YBCO reaction and have been discussed elsewhere[1]. This work concluded that the rate of formation of YBCO is governed by the rate of $BaCO_3$ decomposition and the rate at which Y_2O_3 is able to participate in the reaction. This latter primarily determined by the surface area of the Y_2O_3 present. As almost all precursors used to prepare YBCO decompose to their component oxides and carbonates prior to YBCO formation, this conclusion is for the most part also valid when reactants other than oxides and carbonates are present. This information resulted in two changes in the CPS Superconductor YBCO process. First, the heating rate was slowed down to allow a longer dwell time in the temperature regime where $BaCO_3$ becomes unstable (750°C to 900°C). Second, the

---

[1]L.J. Klemptner, J.D. Hodge, and C. Hubbard, "Phase Formation of Yttrium Barium Cuprate", presented at 92nd Annual American Ceramic Society Meeting, Dallas, TX, April 24, 1990.

J.D. Hodge and L.J. Klemptner, "Preparation of High Quality Yttrium Barium Cuprate Powders Using Solid State Reactions", presented at 92nd Annual American Ceramic Society Meeting, Dallas, TX, April 25, 1990.

calcination atmosphere was changed from ambient air to air in which the CO_2 level was reduced to 2 ppm. Both of these changes served to encourage the decomposition of $BaCO_3$ below the temperature at which YBCO begins to form. However, the longer dwell times at lower temperature also accelerated the unwanted reaction between CuO and Y_2O_3 to form $Y_2Cu_2O_5$ which cannot be removed by subsequent calcination. This problem was alleviated by reducing the surface area of the Y_2O_3 starting material and, consequently, suppressing the reaction between CuO and Y_2O_3 until later on in the calcination process when sufficient BaO became available to form YBCO. Figure 2.7 and Figure 2.8 compare the x-ray diffraction patterns of the YBCO produced before and after these process improvements. Table 2.1 compares Leco carbon analyses of powder produced before and after the implementation of these process changes.

Table 2.1 Carbon level comparisons of various CPS Superconductor YBCO powders

	wt.% carbon
Previous process	0.225
Process w/reduced CO_2	0.132
Process w/reduced CO_2 & low temperature dwell	0.035

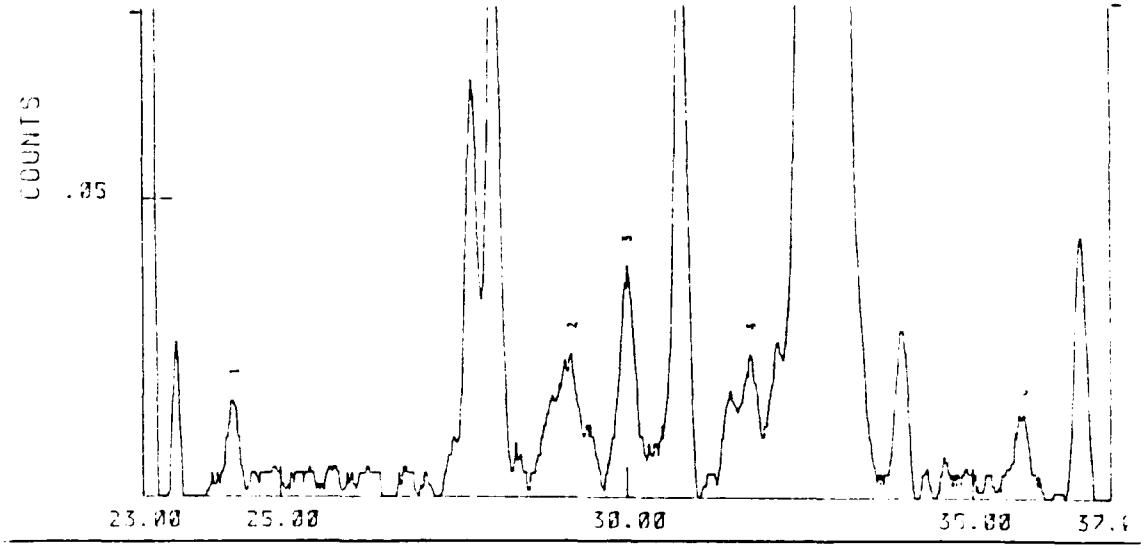

Figure 2.7 X-ray diffraction pattern of YBCO calcined prior to recent process changes.

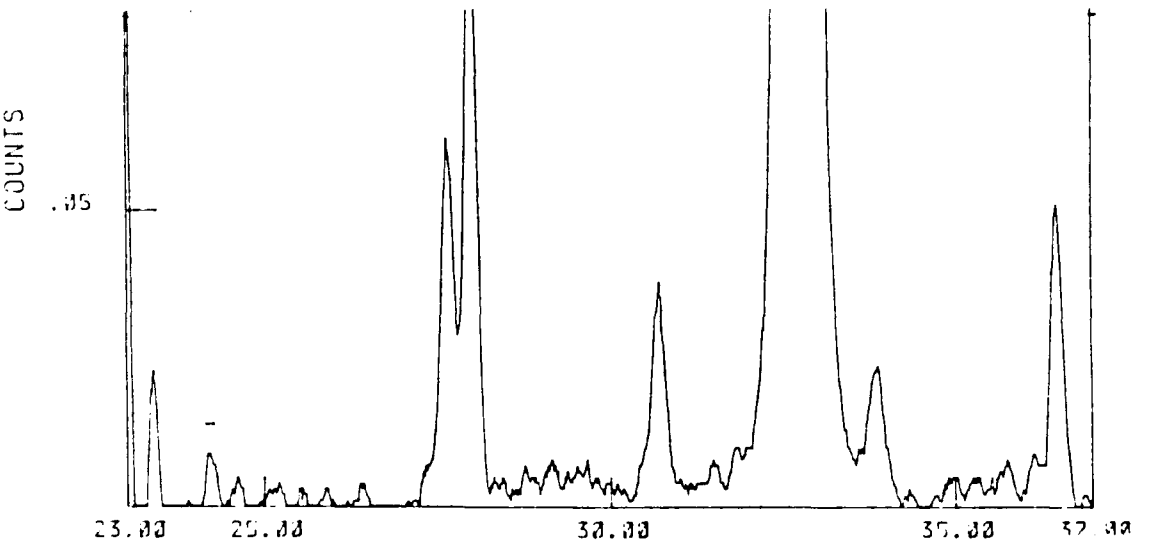

Figure 2.8 X-ray diffraction pattern of YBCO calcined with low temperature dwell and reduced CO_2 pressure.

2.2. Fiber Spinning

Dana Eagles, George Bakis, and Wes Ishida
Albany International Research Corporation

Fiber spinning efforts for the ninth quarter focused on supplying superconducting ceramic green fibers and braids and designing a winder to meet the needs of green fiber spooling. An HDPE formulation was found to which processed well with 60 volume percent YBCO and was used to produce fiber from various YBCO powders. A spin with the standard HDPE formulation at 50 volume percent solids loading was conducted with BiSCCO powder. Two 68 filament flat braids were produced using uncoated and coated YBCO green fiber. Detailed drawings of the winder were completed and fabrication of the machine was initiated.

2.2.1. Melt Spinning of Superconducting Ceramic Fibers

The first superconducting ceramic spin for this period contained 60 volume percent YBCO powder with an altered HDPE formulation to determine if the previously reported problems associated with 60 volume percent solids loadings could be alleviated. The lot compounded well and produced continuous fiber at diameters of 5, 15 and 50 mil. To determine if this new HDPE formulation was reproducible with 60 volume percent solids loadings, a second blend was made with YBCO. The lot compounded similarly to the previous 60 volume percent evaluation and was successfully spun into 5, 10 and 20 mil diameter fiber. Although 60 volume percent solids loading blends process with more difficulty than the standard 50 volume percent blends, the benefits obtained in downstream processing resulted in the

60 volume percent, modified HDPE formulation as the new standard for YBCO green fibers.

The both HDPE formulations were used to compound lots of 50 volume percent YBCO which was doped with excess 211 material. Both lots compounded well and were spun into 5, 10, 15, 20 and 50 mil diameter green fiber.

The final superconducting ceramic spin for this period involved a 50 volume standard HDPE formulation with BiSCCO powder. The powder compounded well but the blend could not fabricate continuous fiber thinner than 10 mil diameter. Attempts to produce 5 mil fiber were unsuccessful as the 5 mil dies appeared to clog before any extrudate resulted. In an attempt to produce 7 mil diameter fiber, approximately 50 ft of 7 mil diameter fiber was produced before the 7 mil die clogged. Since continuous 10 mil fiber was possible, the remainder of the blend was converted to 10 mil fiber.

2.2.2. Winder Design

A filament winder dedicated to the specific needs of green fiber spooling has been needed for some time. In early September, the design, begun in June, was finalized. To address the needs for very low winding tensions, the winder will be speed rather than tension controlled. The yarn speed sensor will be a photoelectric encoder mounted on a common shaft with the low inertia filament guide wheel supported by a custom-designed air bearing. The output from this sensor will input to the spindle motor controller which will adjust the rotational speed of the spool to maintain a constant preset filament velocity. The spool itself will be traversed to

eliminate side-to-side tension cycles as the filament moves from flange to flange across the barrel of the spool. The Uhing drive provides an adjustable traverse span and rate to accommodate different filament diameters and changing spool dimensions resulting from repetitive spool utilization.

The detailed or "working" drawings were completed and supplied to the machine shop by sub-assembly so as to minimize the delay in starting fabrication. Many of the first parts were finished before the last of the sub-assembly drawings were submitted. The only purchased part still on back order is the secondary gearbox which drives the Uhing shaft. This unit is presently scheduled to be shipped from the factory in October. A delay of up to three weeks will probably not affect the projected completion date of the winder, although the supplier of the gearbox is being closely monitored to ensure on-time delivery.

2.3. Wire and Part Development

David B. Chandler, Daniel Dexter, Matthew J. Neal, Mark V. Parish, Michael Parker, and Viren M. Pathare
CPS Superconductor Corporation

While our sintered YBCO wire process definition work has continued, efforts in the area of wire development over the past quarter have focussed primarily on the enhancement of critical current densities over that obtained with our sintered wire. To this end, we have accelerated both our study of the continuous melt-texturing of YBCO fiber and wire and our modification of our YBCO sintered wire process to produce mechanically textured BiSCCO ribbon. In addition, melt-texturing of bulk

YBCO parts has also received substantial attention as part of our efforts to produce a trapped flux motor. Each of these efforts will be discussed below.

2.3.1. YBCO Sintered Wire

The YBCO sintered wire process was discussed extensively in the last quarterly report and will be only briefly mentioned here as work in this area has primarily been to clean up loose ends in the final definition of the pilot-scale wire process. In brief, it has been demonstrated that wire/fiber can be continuously produced in diameters ranging from 100 to 500 μm. The sintering facility presently in place can be used for continuous pilot-scale sintered wire production without major modifications, although an improved method of forming a seam in the Nextel™ belt used to carry the fiber/wire through the furnace is needed to prevent damage to the fiber in this area.

As part of a Phase I SBIR program funded by the Army Center for Signal Warfare, on which CPS Superconductor and Foster-Miller Company, Waltham, MA are joint participants, we have extended our fiber technology to the production of wind-and-fire coils for use as high frequency (1 - 30 MHz) antenna components. In this technique, green fiber is wound on a mandrel covered with a fugitive spacer material. During firing, the spacer material burns away, leaving a gap between the mandrel and the wound fiber to accommodate shrinkage during densification. Figure 2.9 shows a section of a typical coil produced in this fashion. Coils up to 9 cm long containing 170 cm of fiber have been produced. Figure 2.10 shows a J_c plot of such a 9 cm coil.

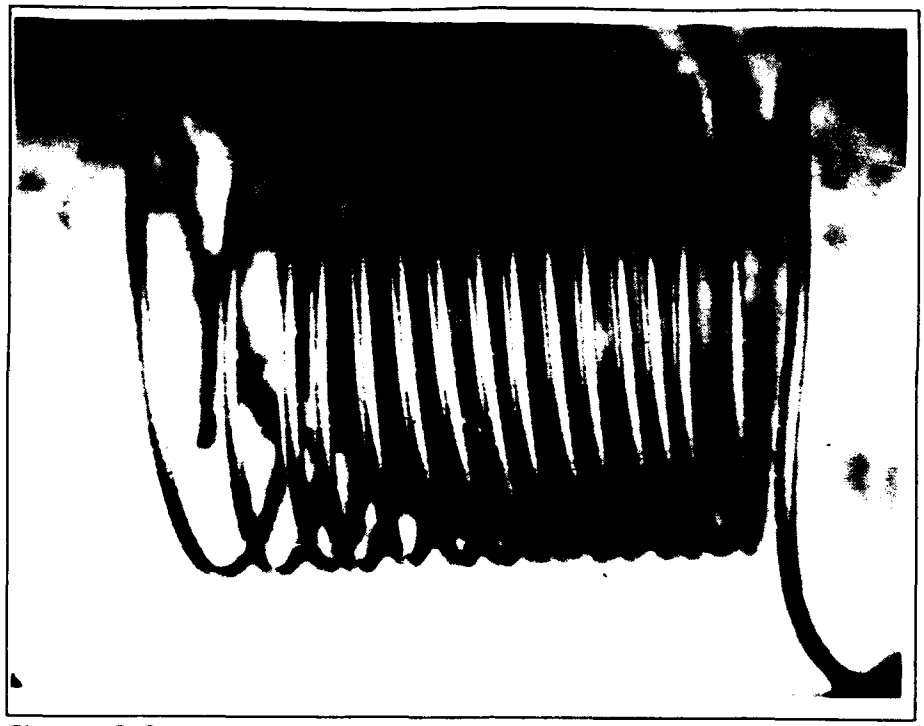

Figure 2.9 Section of wind-and-fire coil produced at CPS Superconductor as a HF antenna component.

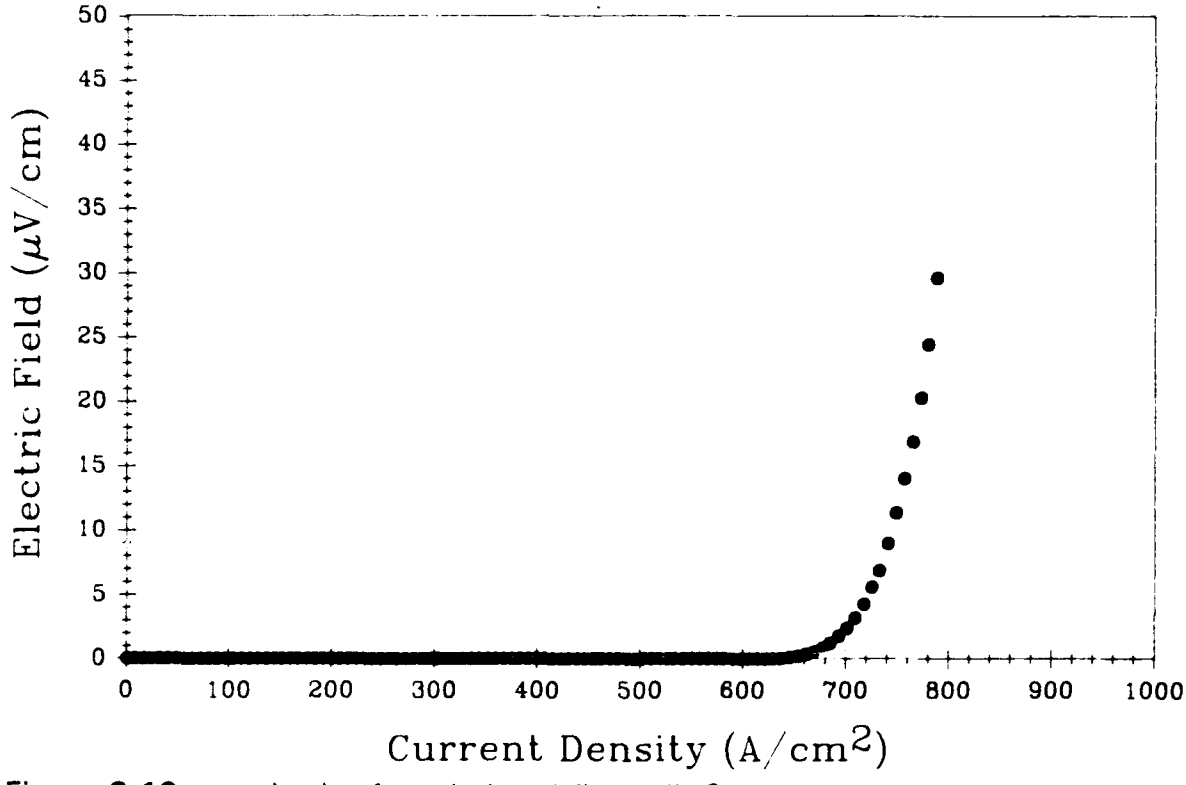

Figure 2.10 J_c plot for wind-and-fire coil, 9 cm long containing 170 cm of fiber.

2.3.2. Melt-Textured YBCO Fibers

The CPS Superconductor fiber melt-texturing process, described in detail in the last quarterly report, involves a simple apparatus in which sintered fibers are slowly pulled through a small "microfurnace" with a 25 mm long hot zone. This microfurnace was fabricated by winding a heating coil around a small diameter ceramic tube. The thermal profile generated by this coil is controlled by cutting slots in the ceramic tube to expose the interior of the furnace to direct radiation of the element in areas where higher temperatures are desired. In the rather crude first generation furnace, temperature was controlled using a variac. Most of the experimental results to be discussed in this report have been conducted with a peak temperature of around 1100°C and a temperature gradient through the peritectic of 150°C/cm. During the past quarter, we have begun to explore the processing "envelope" for fiber melt-texturing by examining both fiber traverse rates and fiber diameter, as well as investigating the feasibility of melt-texturing metallized fibers. Last quarter, we reported that 250 to 375 μm diameter fibers had been successfully melt textured at rates between 1.3 and 4.2 mm/hr. This past quarter, fibers have been melt-textured at rates up to 12.6 mm/hr with no serious degradation in the apparent degree of texture in the microstructure. Figure 2.11 and Figure 2.12 compare microstructures of fibers textured at 4.2 mm/hr and 12.6 mm/hr. We have also successfully textured fibers down to 100 μm in diameter (this being the practical lower limit for handling fibers in our present apparatus), and have observed no

Figure 2.11 Longitudinal section of fiber textured at 4.2 mm/hr.

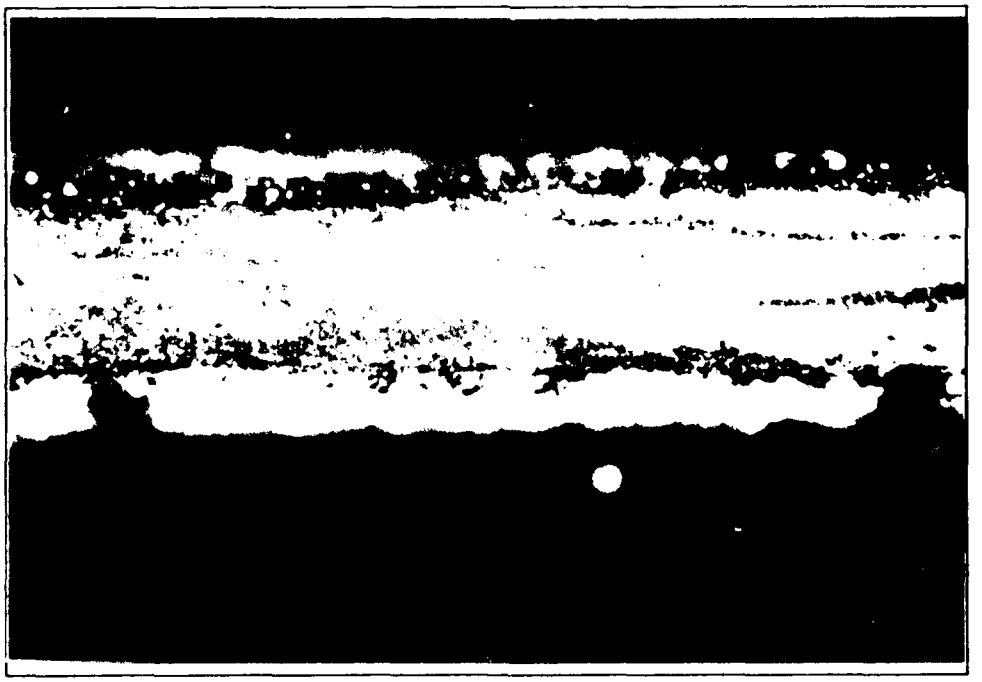

Figure 2.12 Longitudinal section of fiber textured at 12.6 mm/hr.

difference in microstructure between this diameter and the larger diameter fibers more commonly used in this work.

We have also attempted to melt-texture fibers which have been previously co-fired with a 70Ag-30Pd coating (selected so as to be sufficiently refractory to survive the temperatures required in the melt-texturing process). Melt-textured microstructures were successfully produced with these fibers, but the Ag/Pd coating on the fiber was severely degraded. This observation is consistent with earlier studies at CPS Superconductor of interactions between Ag/Pd alloys and YBCO at temperatures below the peritectic[2] where the presence of palladium resulted in the partial decomposition of the YBCO to barium cuprate and 211. Work at Oak Ridge National Labs suggests that this reaction is due to the formation of a Pd/Cu alloy which depletes the YBCO of CuO[3]. We are continuing to study this reaction as it occurs in the melt texturing process.

Critical current density versus magnetic field data on melt-textured fibers are shown in Figure 2.13. This figure compares normal sintered wire with melt-textured fiber produced at two different speeds and also data for fibers melt-textured with a Ag/Pd coating. Note that the upper values for J_c in the figure ($\sim$15,000 A/cm^2) represent the present upper limit for measurement at CPS Superconductor and not the maximum J_c value for the samples. We have purchased a 100 A DC current source

---

[2]V.M. Pathare and H. Park, "Reactions Between Yttrium Barium Cuprate and Silver Palladium Alloys", presented at 92nd Annual American Ceramic Society Meeting, Dallas, TX, April 25, 1990.

[3]T. Schaffhauser, private communication, October 5, 1990.

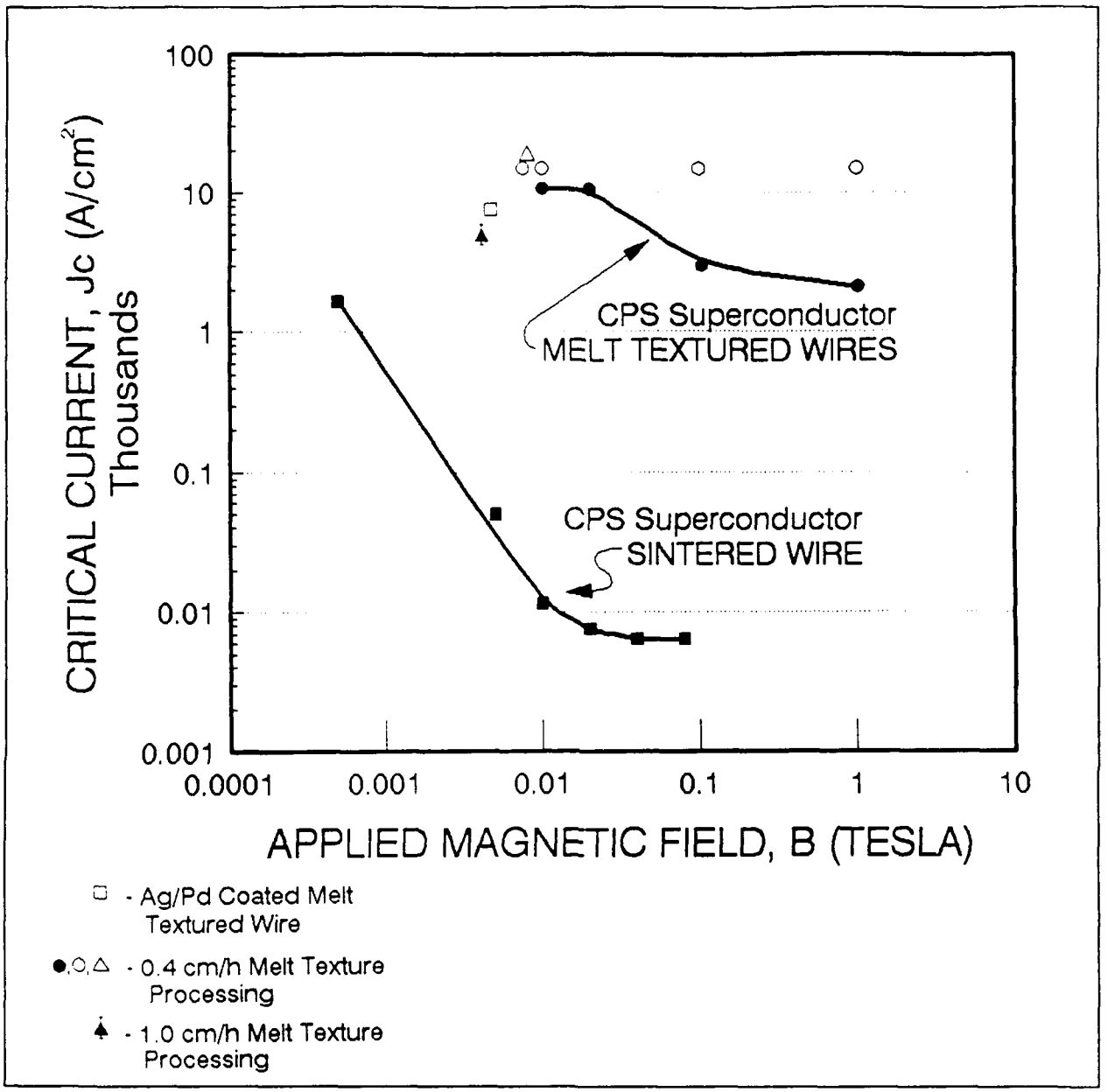

Figure 2.13 Critical current versus magnetic field data for a variety of melt-textured fibers.

(our present limit is 10 A) and are installing it into our electrical characterization facility to enhance our measurement capabilities. In addition, we have submitted samples to NIST-Boulder and Oak Ridge National Laboratory for more extensive characterization at higher magnetic fields and lower temperatures.

Recognizing that temperature and temperature gradient control on the "microfurnace" constructed to demonstrate the principle of continuous fiber melt-texturing was too crude to effectively quantify this process, we have designed and constructed a second-generation microfurnace which will allow us to precisely control the peak process temperature. In addition, the furnace has been designed with three separate heating zones, all individually controlled, which will allow us to control the magnitude of the thermal gradient the fiber experiences as it traverses the peritectic. This furnace is currently being qualified and we will report on the results obtained using it next quarter.

The major issues with the fiber melt-texturing process are the slow rate at which it presently proceeds and the non-uniformity of electrical properties along the length of a melt-textured fiber. We expect that work in the up-coming quarter with more precise temperature control and fiber handling will allow us to more precisely define the maximum rate at which melt-textured material can be produced. The non-uniformity of electrical properties issue has been extensively studied this past quarter. Most of our work in this area has centered on the correlation of electrical properties and microstructure. As discussed last quarter, the microstructure of a typical melt-textured fiber is not uniform along its length, both the number and apparent orientation of grains change as a function of position and we have tentatively identified regions with the fewest, high aspect ratio grains as yielding the highest J_c values. Consequently, we have focussed our efforts on a study of the origins of this changing microstructure along the length of a melt-textured fiber. A number of

possibilities are being pursued: 1) The lack of precise temperature control and fiber positioning in the present furnace results in the fiber experiencing a constantly changing temperature and temperature gradient as it traverses the peritectic. As a consequence, the fiber's degree of supercooling and the YBCO nucleation rate is constantly changing. Our new controlled temperature microfurnace should allow us to quantify this effect. 2) As the melt-texturing process is, in effect, a directional solidification process, the possibility for solute segregation exists where impurities accumulate at the crystallization front until a point is reached where they exist in sufficient concentration to pin the front and inhibit further growth. At this point, supercooling ahead of the pinned front increases and a new wave of nucleation and growth occurs. While we see no microstructural evidence for gross segregation, i.e, second phase at boundaries, we will continue to explore the possibility of chemical segregation in the next quarter.

2.3.3. Melt-Textured YBCO Pellets

We have performed extensive studies of the melt-texturing process on pellets to help us to further understand the melt-texturing process as it occurs in the melt-textured fiber process. An additional incentive for this work has also been derived from the need to fabricate melt-textured "magnet replicas" for the trapped flux motor designed by Emerson Electric which will be discussed in a later section. Our studies of melt-texturing in bulk materials have been aimed at identifying optimal thermal cycle and compositional regimes for this process. Specifically, this past quarter's effort has focussed on the effect of excess 211 phase and cooling cycle on the

resultant recrystallized microstructure. In this respect, our primary characterization tool has been optical metallography, although we have begun to characterize the electrical and magnetic properties of these materials.

In a typical experiment, a sample pellet (2.5 cm in diameter), presintered to 930°C, is heated in air to a hyper-peritectic temperature between 1030° and 1100°C and held at that temperature for 12 to 24 minutes. The sample is then rapidly cooled to a temperature where the crystallization process begins. It is the nature of this cooling through the peritectic which has been the primary subject of investigation this past quarter. Two types of furnaces have been used, a box furnace which subjects the crystallizing sample to an isothermal environment, and a tube furnace which imposes a 1°/cm to 3°/cm thermal gradient on the sample. Melt-texturing experiments have been carried out in both furnaces using samples having compositions ranging from 0% to 22% excess 211. The thermal cycles investigated have included both slow ramps through the peritectic temperature and isothermal experiments where samples are quenched through the peritectic and held at a fixed temperature for a fixed period of time.

Observations of samples recrystallized in an isothermal environment indicates that the microstructures obtained are consistent with what would be predicted by classical nucleation and growth theory. In isothermal experiments, samples which are quenched to a lower temperature (greater supercooling), recrystallize with a smaller grain size than those which are recrystallized with a lower degree of supercooling. Note that as these samples are crystallized in an isothermal

environment, these recrystallized grains are not textured, but are randomly oriented. It was observed in this set of experiments that the nucleation rate of YBCO from the peritectic mixture is extremely slow and that a substantial supercooling is required to achieve complete crystallization. For example, a 25 g sample quenched from 1065°C to 1000°C (15°C below the peritectic in air) and annealed at this latter temperature for 12 hours will contain only 2-3 YBCO grains approximately 2-3 mm in diameter with the bulk of the sample consisting of a mixture of 211 and barium cuprate, i.e., a quenched peritectic mixture. However, a 25 g sample quenched to 985°C (30°C below the peritectic) will be fully crystallized with an average grain size of 1-2 mm. Again consistent with nucleation and growth theory, the largest YBCO grains (1 cm in diameter) were obtained when samples were slowly cooled (1°C/hour) through the 985° to 1000°C temperature range.

Incorporation of excess 211 into melt texture samples had little apparent effect on the recrystallized grain size, but did affect the nature and distribution of second phase in the sample. In phase pure YBCO samples, peritectic 211 particles are entrapped in growing YBCO grains during recrystallization. This causes the liquid ahead of the crystallization front to become enriched in the peritectic liquid. Ultimately, this enrichment results in $BaCuO_2$ and CuO crystallizing at boundaries upon impingement between neighboring YBCO grains. Figure 2.14 shows a typical example of this type of second phase between impinged YBCO grains. In samples containing excess 211, 211 particles are also entrapped inside growing YBCO grains. However, due to the 211 excess, liquid phase enrichment does not occur ahead of the

Figure 2.14 Second phase present between impinged YBCO grains in a phase pure melt-textured pellet.

crystallization front. As a consequence, no precipitation of barium and/or copper compounds is observed at grain boundaries in these materials. Some segregation of 211 does occur when this material is present in excess. Regions of aggregated 211 particles were observed in all samples which contained excess 211. These 211 aggregations were universally isolated at three grain junctions with the size and number of the aggregations being proportional to the amount of 211 excess in the sample.

Samples cooled in a slight thermal gradient showed a markedly different microstructure. While crystallization occurred in the same temperature ranges as were observed in the isothermal samples, the presence of the thermal gradient lent directionality to the growth of the YBCO crystals, as expected. However, two

distinctive modes of crystallization were observed. YBCO nuclei initially formed at the cool end of the sample grew into large highly directional YBCO grains. However, unlike samples treated isothermally, these crystallizing YBCO grains trapped very little 211 as they grew. Consequently, the concentration of 211 particles ahead of the crystallization front increases. At the point at which the isolated 211 particles come into contact with one another, the mode of crystallization changes. The directional growth of YBCO ceases, replaced by a spherulitic-like crystallization of YBCO in the region of high 211 concentration. The boundary between these different crystallization modes is clearly seen in Figure 2.15. This spherulitic crystallization is entraps most of the 211 particles, although significant amounts of this material ends up at triple points between impinged spherulites. It is believed that this change in crystallization modes is consequence of the increased 211 concentration is this region which pins the existing crystallization fronts, preventing their growth. With crystallization terminated, cooling in the uncrystallized region continues until a critical supercooling is reached where new YBCO nuclei are able to sweep through the aggregation of 211 particles. The fact that segregation of 211 particles occurs ahead of the YBCO front is believed to be an artifact of the small thermal gradient imposed upon these bulk samples[4]. A study of this phenomenon is continuing.

---

[4]In melt-textured fibers, as noted earlier, where a significantly larger thermal gradient exists, no segregation of 211 occurs.

Figure 2.15 Interface between directional crystallization and spherulitic crystallization zones in melt-textured YBCO.

2.3.4. BiSCCO Wire Development

Another major effort during the past quarter has been the adaptation of the CPS Superconductor sintered wire process to the production of textured BiSCCO ribbon wire. Briefly, our concept is to produce silver-coated green BiSCCO fiber, sinter this fiber at a temperature high enough to densify the Ag coating, roll this "presintered" wire into thin ribbon to induce orientation in the BiSCCO, and subsequently anneal this ribbon to optimize the material's superconducting properties.

The feasibility of this procedure has been demonstrated in the past quarter. Using the BiSCCO powder produced in-house (see Section 2.2), 125 μm and 250 μm diameter fibers were spun, coated, and pre-sintered using the same continuous

process facilities developed for YBCO fiber/wire. Unlike the sintered YBCO wire which are typically coated with sufficient silver to produce a 10 to 20 μm thick fired coating, BiSCCO fiber was coated with enough silver to produce a 50 μm thick fired coating. This thicker coating was decided upon to allow the fiber to better accommodate the subsequent deformation during rolling.

A set of Contenti Italian rolling mill was purchased to evaluate the rolling behavior of the presintered BiSCCO wire. This mill, consisting of a set of 1.75" diameter rolls with a continuously variable gap, will allow us to evaluate the processing of our presintered wire over a wide variety of mechanical deformations. Figure 2.16 shows a BiSCCO wire, presintered at 830°C, and Figure 2.17 shows this BiSCCO wire after rolling through a 75 μm gap. The mechanical properties of this rolled ribbon are excellent and lengths of up to 5 feet have been produced and spooled onto 2 inch diameter bobbins without fracture. Note that the smallest bobbin which our sintered YBCO wire can be spooled on is 8 inches.

The initial process work described here was performed on non-optimized powder to allow us to evaluate both continuous sintering and rolling. The ribbons produced from this powder were subjected to post-rolling anneals for 48 hours at temperatures between 830° and 850°C in air. All of these samples showed evidence of the formation of gross amounts of liquid phase in this temperature range. Microscopic examination of these samples showed significant degradation. Currently, fibers are being made with optimized powder which will be used to produce similar ribbons for experiments aimed at optimizing the post-fire annealing process.

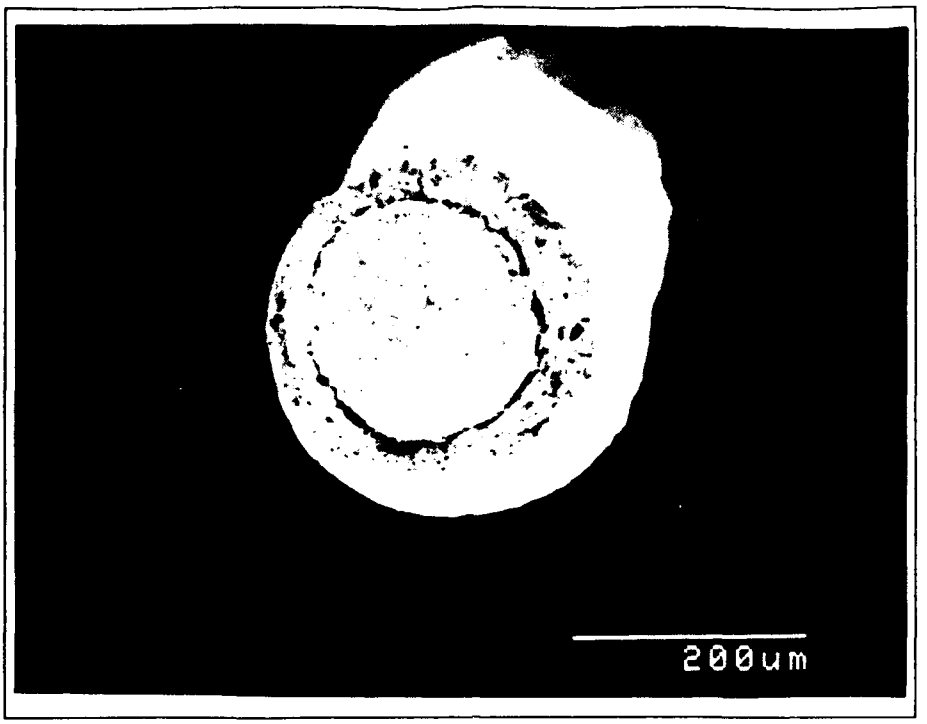

Figure 2.16 Presintered Ag-coated BiSCCO Wire.

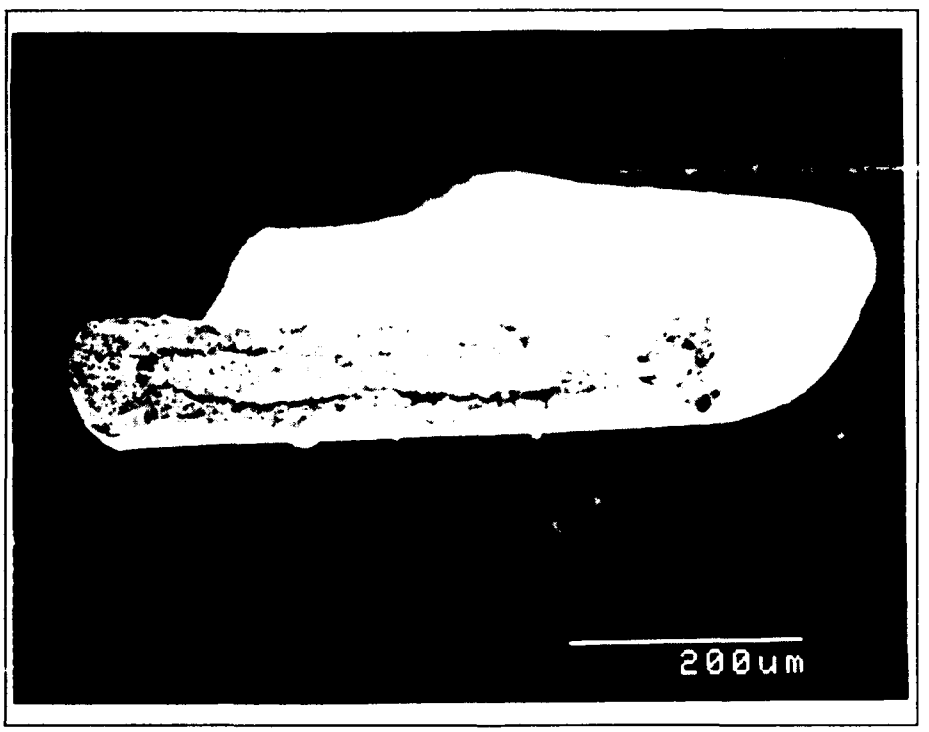

Figure 2.17 Presintered BiSCCO wire after rolling.

2.4. Motor Design and Fabrication

Alan Crapo and Jerry Lloyd
Emerson Motor Company
Mohamed Hilal
University of Wisconsin

The Emerson Motor Division (EMD) of Emerson Electric Company has been designing, building, and testing motors to be used with HTSC materials. In designing and building HTSC motors, there are two major objectives. The first is to develop a motor or motors which will test the HTSC wire produced by CPS Superconductor, and to verify that the wire meets its performance goals in a real motor. The second major objective is to design and build a motor or motors that are optimized to take advantage of the characteristics of the newly developed HTSC materials.

A homopolar DC motor has been designed and built to test HTSC wire wound into field coils. Details of the design have been reported in previous quarterly and annual reports. While CPS Superconductor is working on HTSC wire for the homopolar motor field windings, we have been testing the motor with copper field windings. Test results are reported.

We have also been investigating motor concepts which are based on trapping flux with bulk HTSC materials. We have built a brushless DC motor which will test bulk rings of HTSC material that will trap flux in the rotor. The motor design and theory of operation are presented.

2.4.1. Iron Core Homopolar Motor

In previous reports, we have presented the design and performance calculations of the homopolar DC motor. HTSC field windings are not yet available, so the motor was first wound with copper field windings. A cross section of the homopolar motor is shown in Figure 2.18. We have been testing the copper field winding version of the motor.

The first thing we tested when the homopolar motor was assembled was the flux through the rotor between the brushes. Using one of the six field coils as a search coil connected to a fluxmeter, we measured the flux produced by the other coils. The results are plotted in Figure 2.19. At the designed level of 575 Ampere turns, the measured flux of 0.0130 Webers is within 1% of the 0.0129 Webers calculated from the finite element model.

Most of the error at the other operating points is due to the error in the model of the B-H characteristics of the steel in the finite element program.

Once the brushes were run in, we measured the back EMF at 1500 RPM as a function of current in the field coils. The curve is plotted in Figure 2.20. The measured back EMF of 0.646 Volts is 7% higher than the calculated level of 0.603 Volts.

While the motor was running at 1500 RPM in room temperature air, we measured the voltage drop in the brushes and motor leads versus current. The results are shown in Figure 2.21. The voltage drops are about as large as the back EMF. That means this motor cannot have high efficiency with this simple current collection

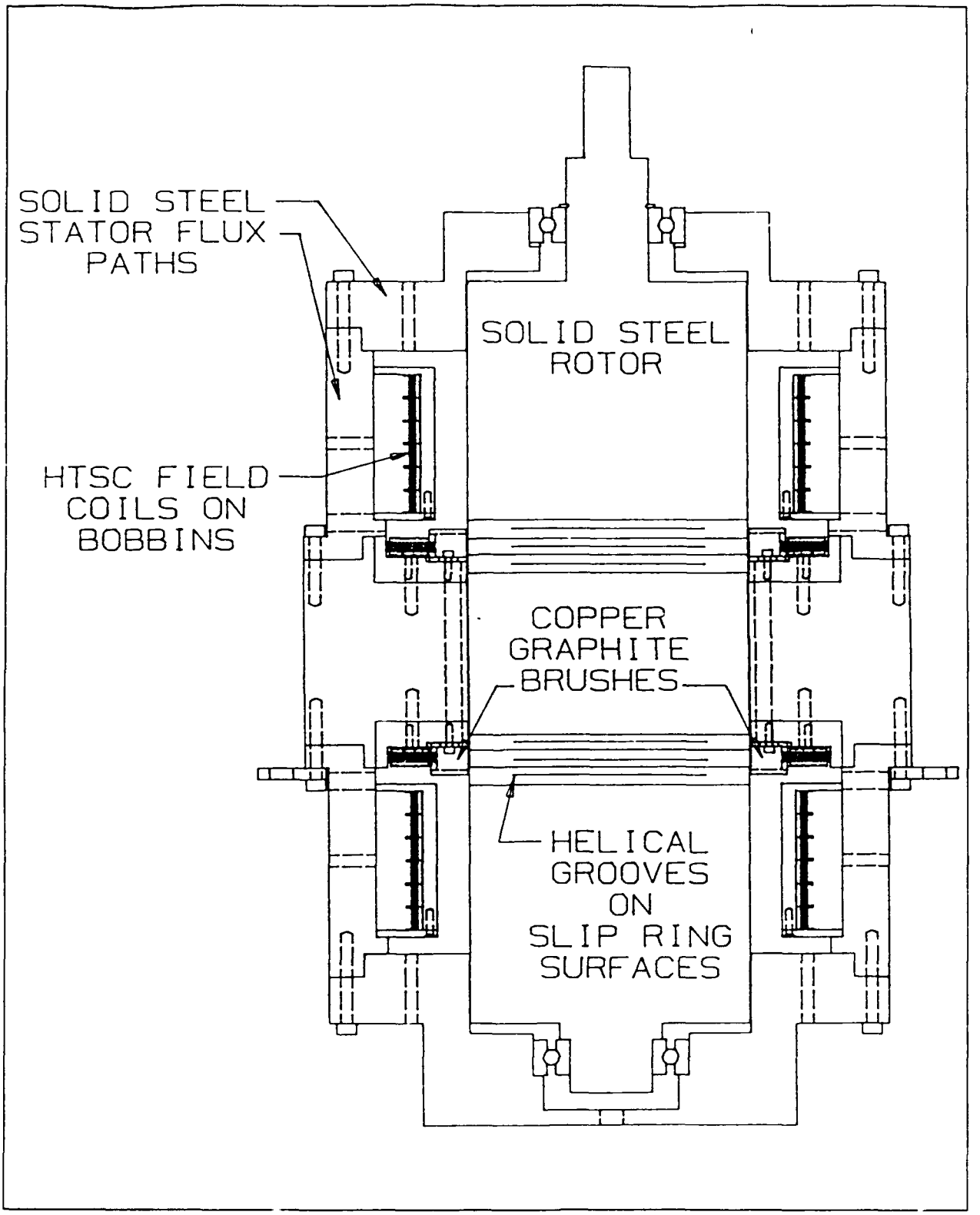

Figure 2.18 Cross section of the steel core homopolar DC motor with HTSC field windings.

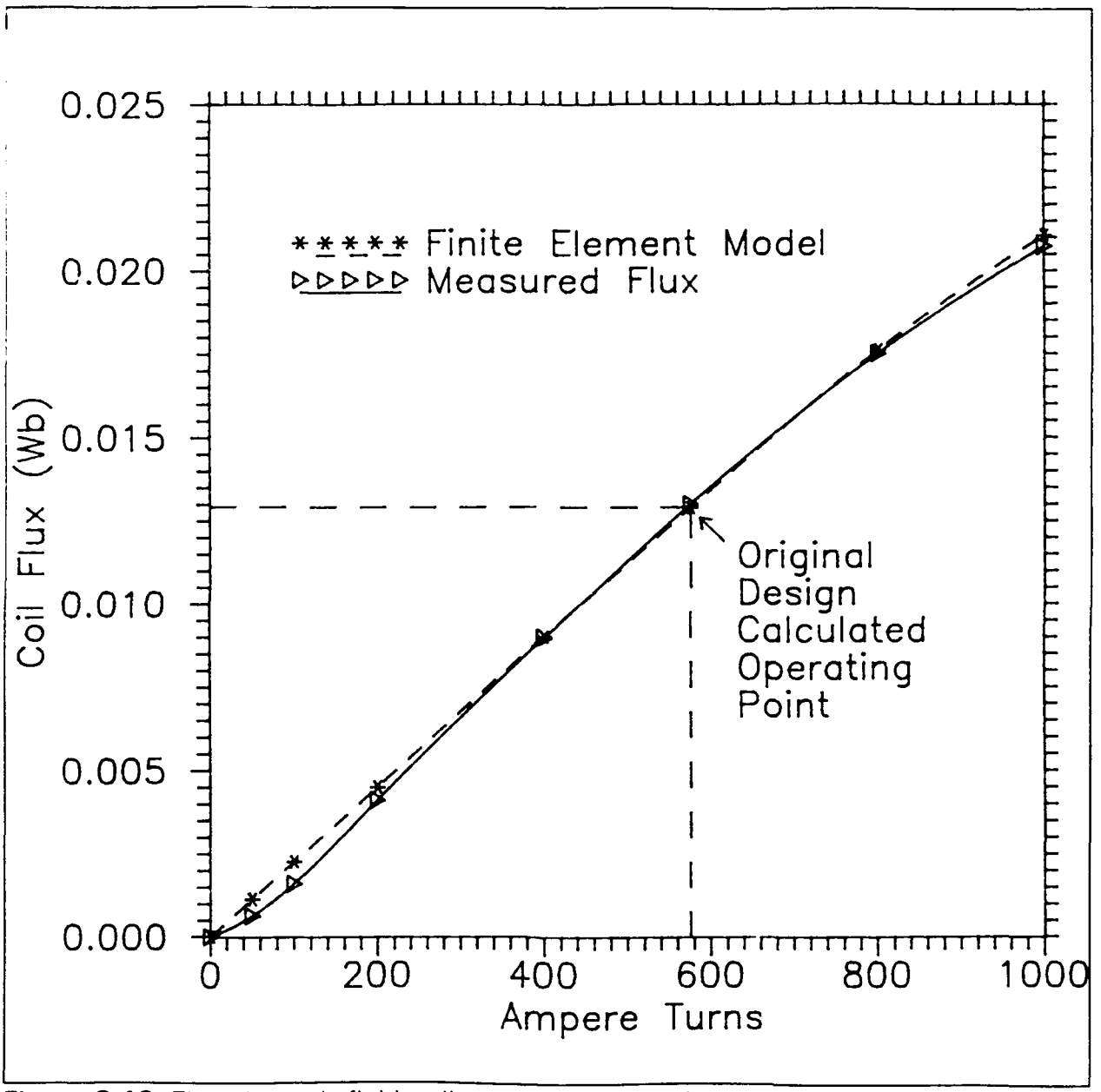

Figure 2.19 Flux through field coil versus field coil Ampere turns.

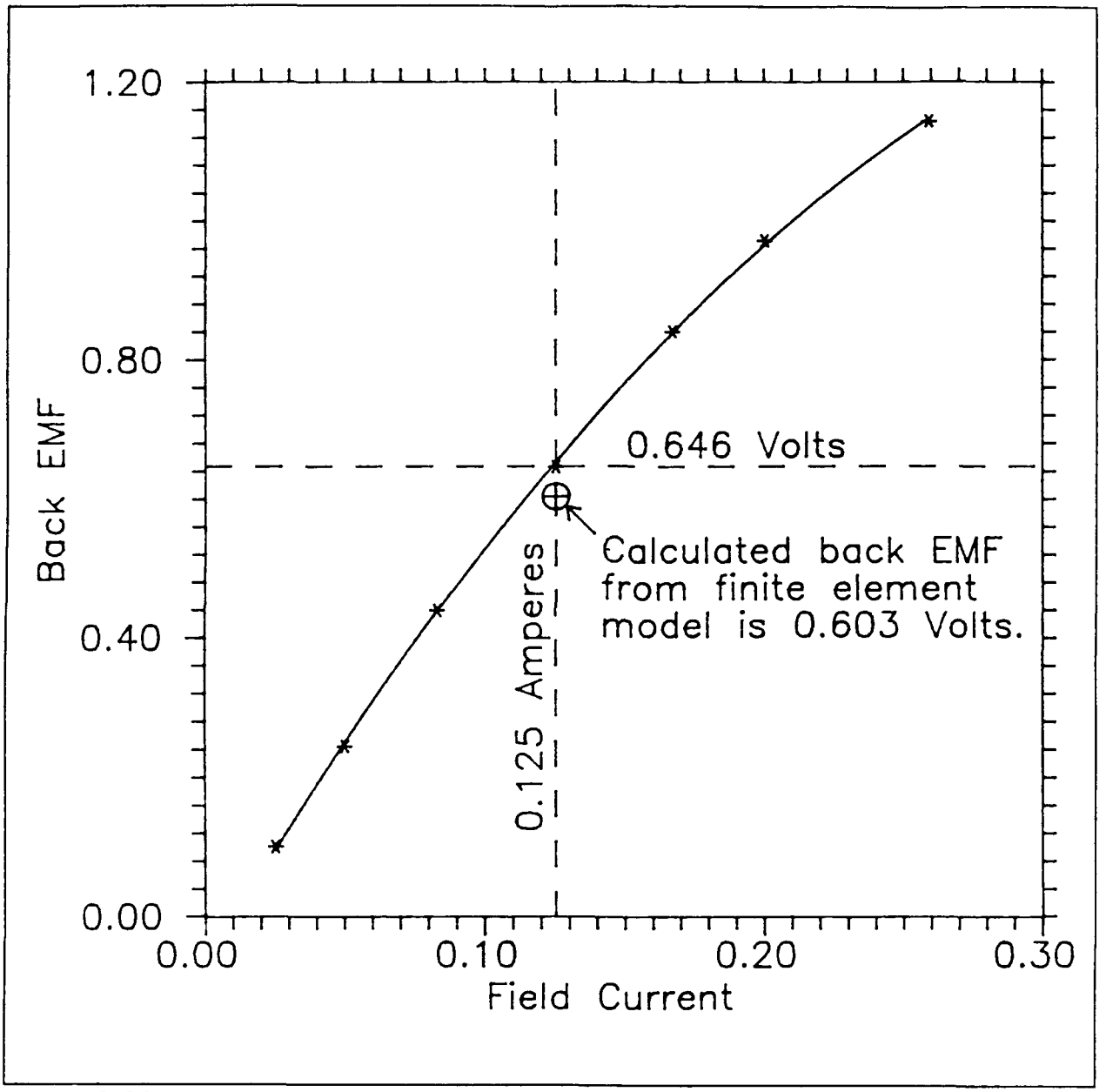

Figure 2.20 Back EMF of homopolar DC motor versus field current at 1500 RPM. Designed field current of 0.125 Amperes is marked.

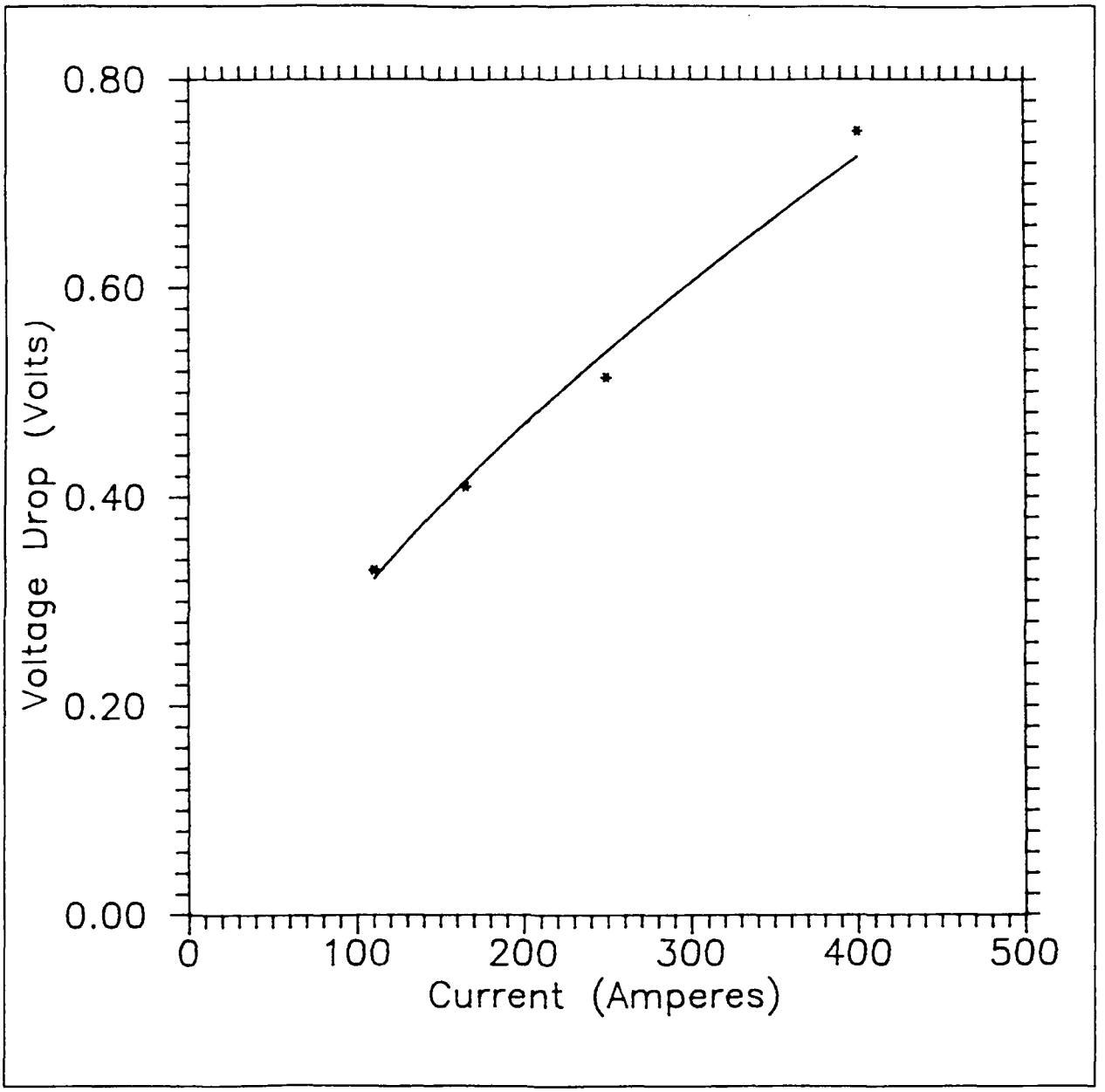

Figure 2.21 Voltage drop across brushes and leads versus current in homopolar DC motor in room temperature air.

system of copper graphite brushes and grooved steel slip rings.

The brush and bearing friction measured in room temperature air at low speed was 1.36 Newton-meters.

The motor was then run at no load in room temperature air, and then later tested in liquid nitrogen. No load speed and current versus applied voltage are shown for room temperature air and for liquid nitrogen in Figure 2.22. The no load current was fairly constant with speed in air, but viscous losses loaded the motor down in liquid nitrogen, requiring more current to produce the additional torque at higher voltages and speeds. Of course, the motor ran slower in liquid nitrogen for the same voltage.

We also loaded the motor with a brake and measured the torque, speed, voltage, and current at various load points.

Table 2.2: Homopolar motor performance data

Torque (N-m)	Speed (RPM)	Volts (V)	Amperes (A)	Output (Watts)	Input (Watts)	Efficiency (%)
1.13	295	0.83	450	35	374	9.3
1.13	2100	2.0	950	249	1900	13.1
2.26	325	1.0	710	77	710	10.8
2.26	1970	2.0	1240	466	2480	18.8
3.16	350	1.4	990	116	1386	8.4
3.16	1300	2.0	1400	430	2800	15.4

With the electrical losses in the brushes, and the viscous losses in the liquid nitrogen, the efficiency of this motor is not very good. As we have pointed out from

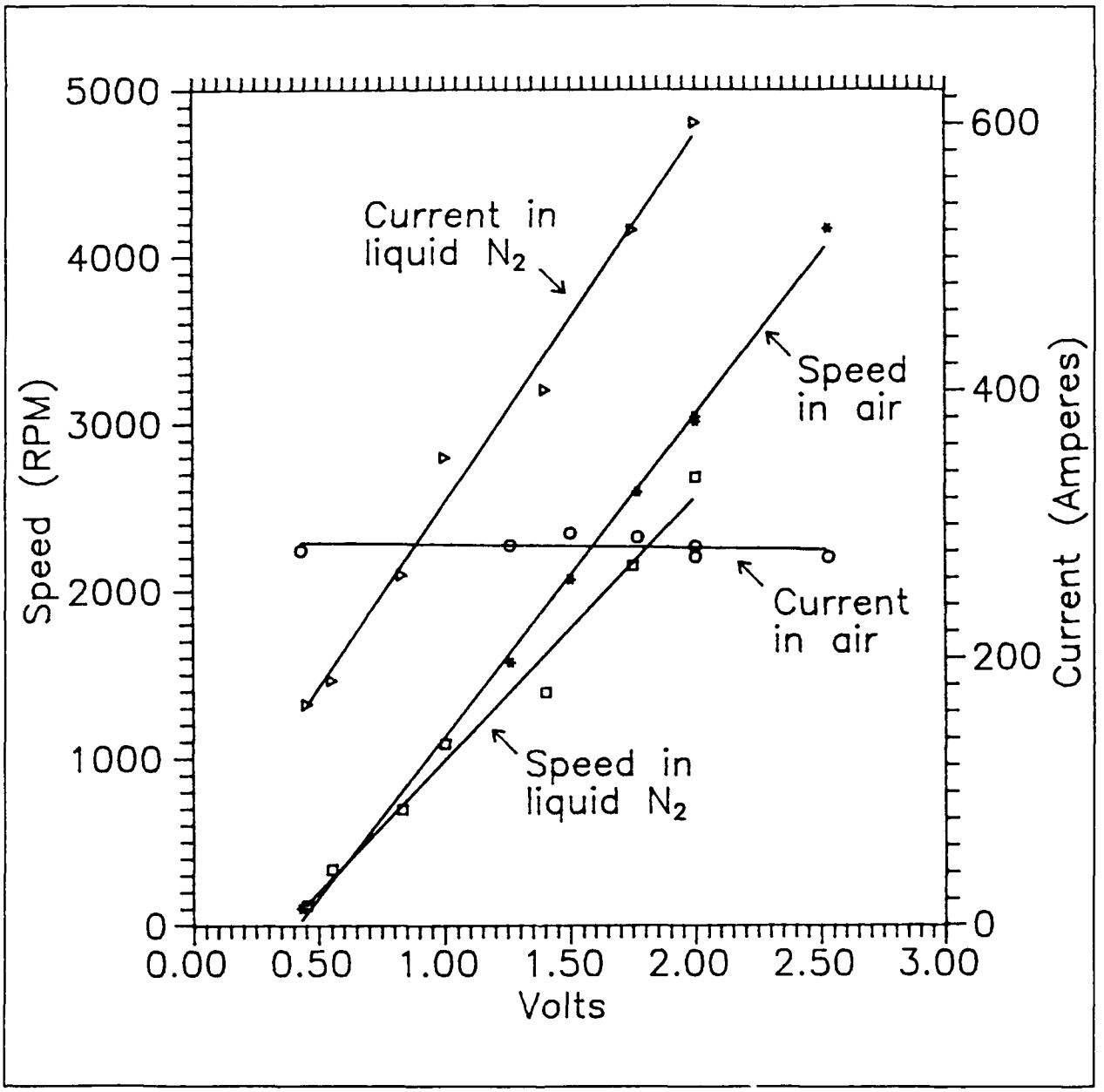

Figure 2.22 No load speed and current versus voltage measured in room temperature air and liquid nitrogen.

the beginning, the main purpose of this motor is to test HTSC wire, not to represent an optimum motor design. The motor will work quite nicely for testing HTSC wire. CPS Superconductor is working on a multifilament braid type sintered wire that should be promising to wind this motor with. When the wire has been wound on bobbins, we will then test the homopolar motor again with the superconductor field windings.

2.4.2. Brushless DC "Trapped Flux" HTSC Motor

In the last two reports, we introduced the concepts of trapping flux in bulk superconductors to make brushless DC motors. CPS Superconductor has trapped up to 0.03 Tesla (300 Gauss) in an HTSC disc, but high Ampere turns within the superconductor are required to trap even 0.03 Tesla (300 Gauss) in the superconductor. When iron is used in the magnetic circuit, the Ampere turns to produce high flux density is greatly reduced. Since 0.03 Tesla (300 Gauss) is too low of an operating flux density for any practical motor, we designed a motor with steel flux paths and small air gaps to take advantage of steels high permeability. Superconducting rings around a steel pole would trap fields in the steel with persistent current around the superconducting loop. Figure 2.23 shows the rotor of the trapped flux motor and Figure 2.24 shows the stator.

This prototype motor works by first cooling the stator and energizing the stator windings with DC current to impose a magnetic field on the rotor. The superconducting rings are then cooled. When the stator field is removed, currents will be induced in the rings to maintain as much as possible, the original field at the time at cooling. Once this "permanent magnet" field is established, the motor can

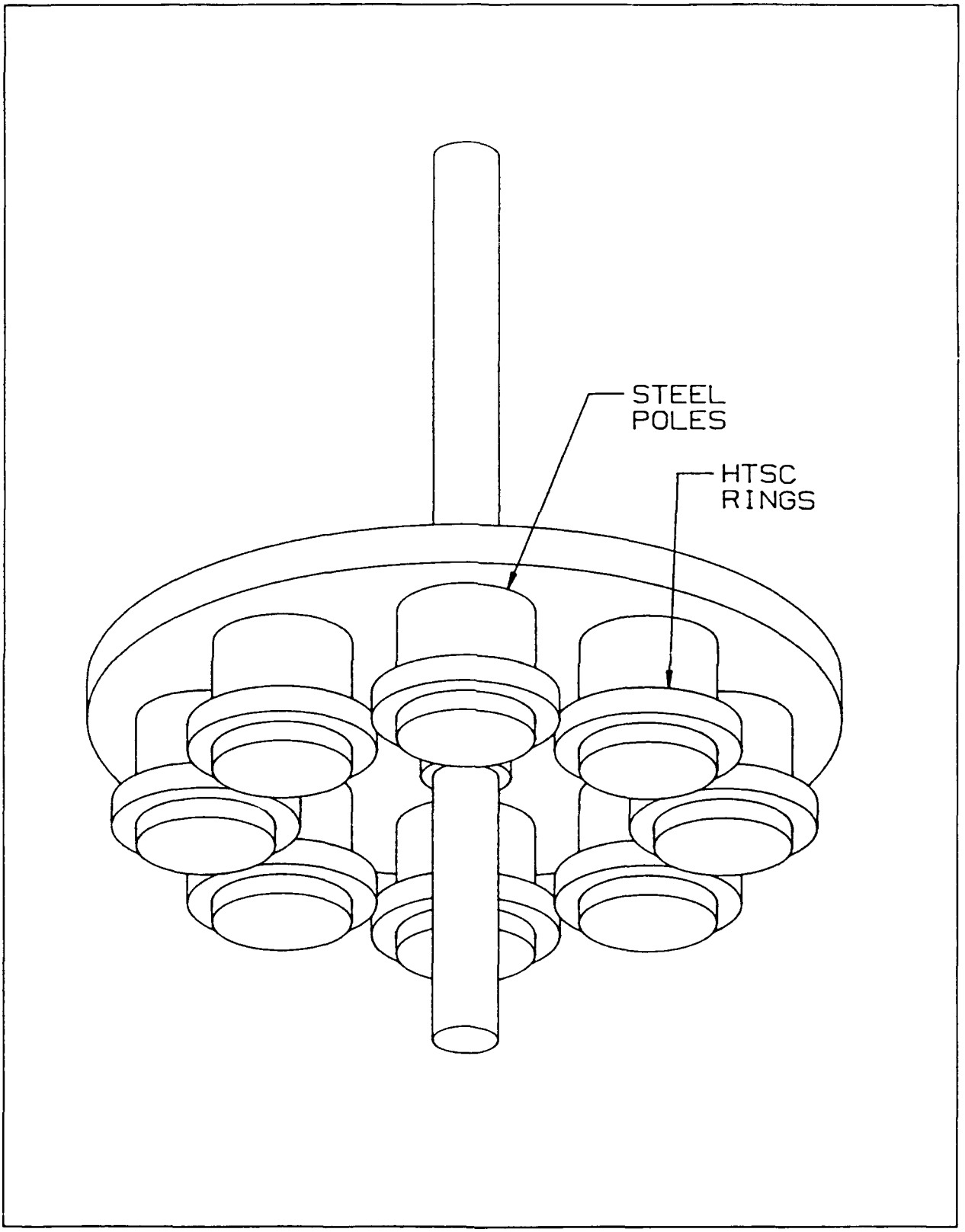

Figure 2.23 Rotor of the brushless DC trapped flux motor.

then operate as a brushless DC motor. The high permeability of the steel allows us to have high flux density with much lower current density in the superconductor.

Trapping fields in a disc requires currents circulating within the grains of the disc. Larger grains can circulate more current and trap more flux. Transport current between grains does not need to be very good to circulate current and trap flux within a grain. When a current ring is around a steel pole, the Ampere turns required to produce the flux in the steel is reduced by a factor of 10 to 100 or more. Even though transport J_c around the ring can be 10 to 100 times lower than the intergranular J_c, there are significant manufacturing challenges in getting 1000 Amperes/cm^2 transport J_c around the loop.

We have been using finite element modeling to analyze the current density required in a magnetic field for the motor to work. Figure 2.25 shows a flux plot of a side view model of one pole of the motor. The flux density in the steel pole is 1.0 Tesla. with a stator slot current density of 1550 Amperes/cm^2. The superconductor ring is cooled while the field is maintained through the ring.

With an average current density of 620 Amperes/cm^2 in a field of 0.04 Tesla (400 Gauss) in the superconductor ring, a field of 0.4 Tesla (4000 Gauss) can be maintained in the rotor poles when the stator current is removed. The resulting flux plot is shown in Figure 2.26.

If the stator windings are then energized as a brushless DC motor, torque is produced. With currents in the stator windings that correspond to a current density of 155 Amperes/cm^2 in the slot, the torque will be approximately 1.0 Newton-meter.

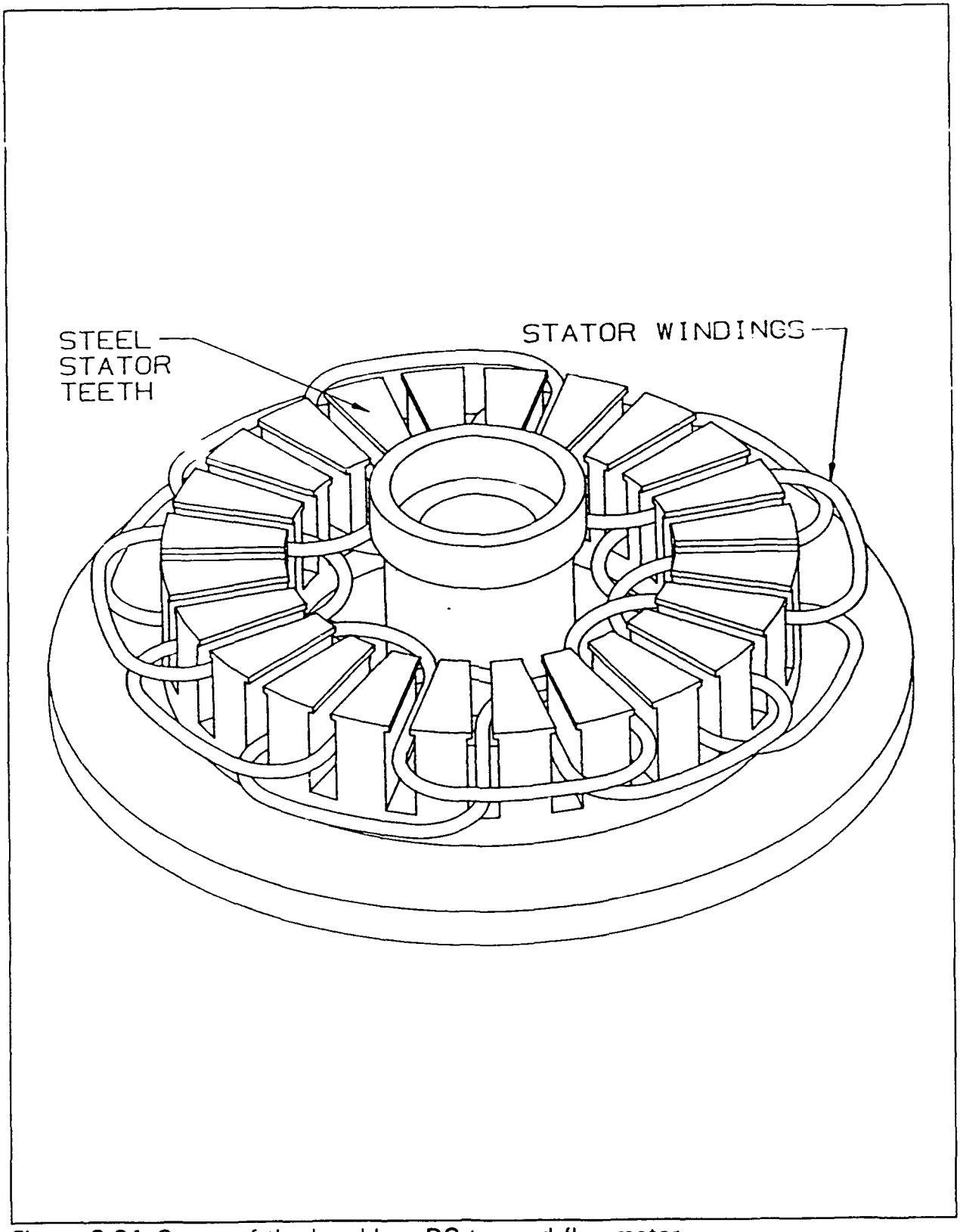

Figure 2.24 Stator of the brushless DC trapped flux motor.

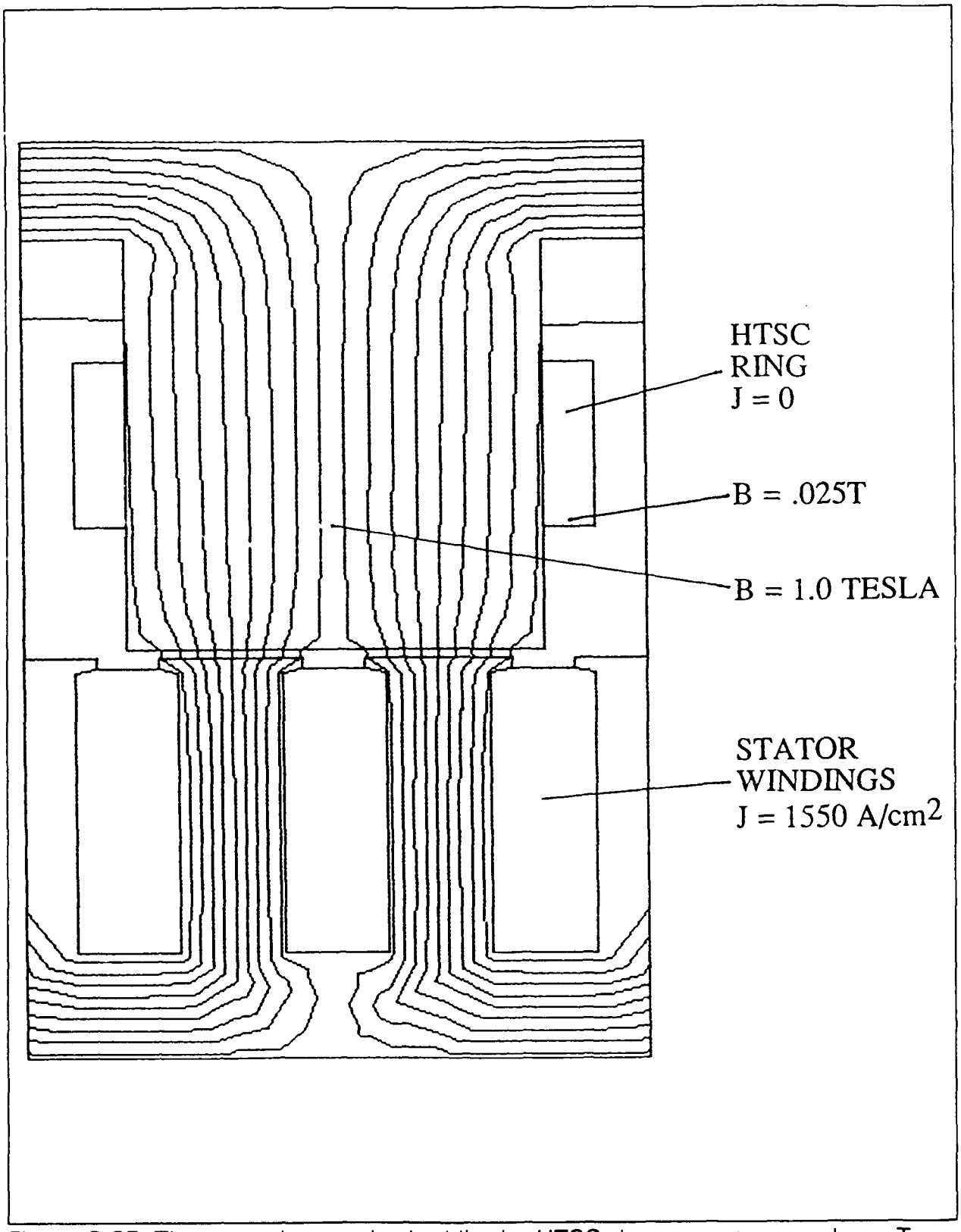

Figure 2.25 The stator is energized while the HTSC rings on rotor are above T_c.

The flux plot is shown in Figure 2.27. Of course, more stator current would produce more torque, and higher J_c will trap more flux and produce more torque.

Our trapped flux brushless DC motor is built and is ready to test HTSC rings. We are waiting for the rings that will be available very soon. Efforts of the next few months will focus on getting the right properties in HTSC rings to make this motor work.

There will be some nice practical advantages to making motors with bulk HTSC material. While there are great difficulties in mass producing ceramic wire, bulk shapes are much easier to make in large quantities. The optimum motor of the future will probably have bulk superconductor materials in the rotor to trap flux, and superconducting wire in the stator to carry high current density.

2.4.3. Motor Activity Summary

We have designed and built a homopolar DC motor that will operate with HTSC field coils submerged in liquid nitrogen. The motor has been built with copper field windings while waiting for the HTSC coils to be available. We have been testing the motor in room temperature air and in liquid nitrogen. The measured flux and back EMF are close to the values predicted by finite element modeling. Viscous losses in liquid nitrogen, and voltage drops in the brushes result in a motor with low efficiency, but still adequate as a test bed for HTSC wire.

We have built a motor with a steel magnetic circuit that will use bulk HTSC rings to trap flux and operate as a brushless DC motor. The motor is built and is ready to test melt textured HTSC rings. Transport J_c values of 600 to 1000

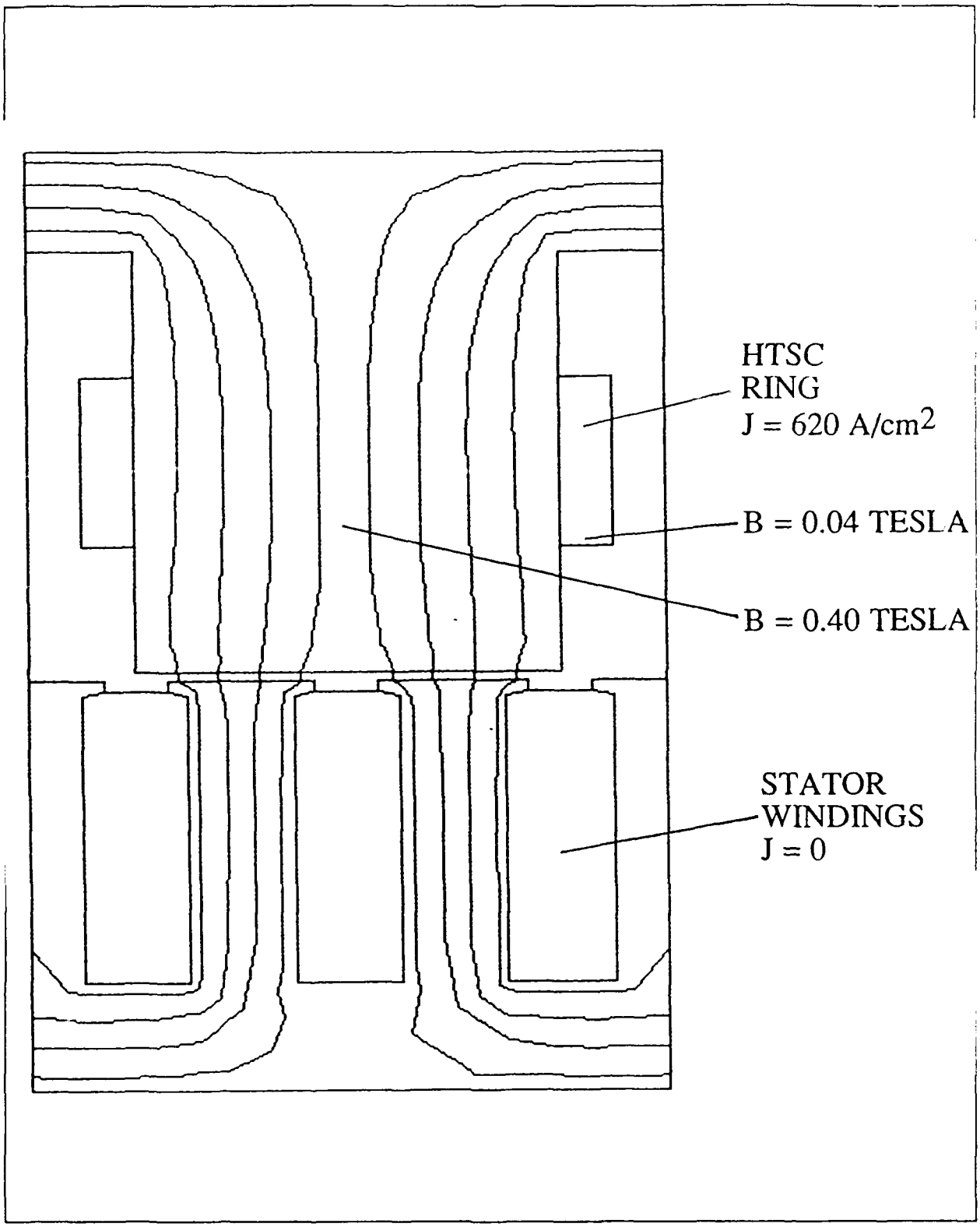

Figure 2.26 Currents in the HTSC rings on the rotor maintain the magnetic field after the stator current is turned off.

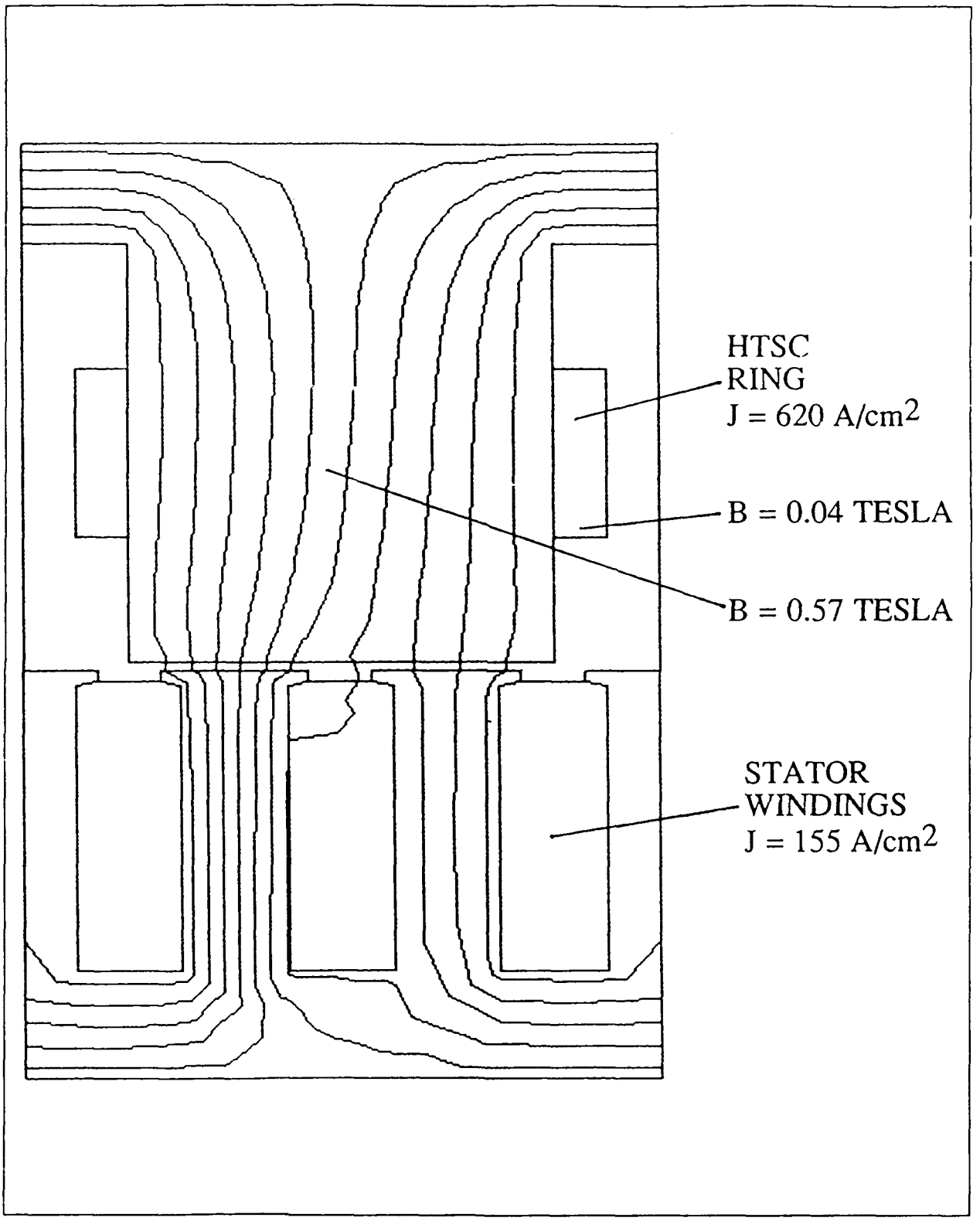

Figure 2.27 Current in the stator windings while the field is trapped in the rotor produces torque.

Amperes/cm^2 should produce substantial torque. We will be testing the motor with HTSC rings in the next few months.

3. GOALS FOR FUTURE REPORTING PERIOD

The coming quarter will see a continuation of our efforts to produce enhanced J_c wire. Two new subcontracts are currently being negotiated subject to the availability of funding. The first is with the HTSC Pilot Center at Oak Ridge National Laboratory. This subcontract will be aimed at quantifying and improving the $YBa_2Cu_3O_{7-x}$ fiber melt-texturing process developed at CPS Superconductor. This Oak Ridge subcontract will give the program access to sophisticated analytical facilities and materials expertise which will greatly enhance our capabilities. The second subcontract under negotiation is with the University of Michigan. This subcontract, which will be led by John Halloran, the principal investigator of the CPS Superconductor/DARPA program until August of this year, will be aimed at achieving an understanding of flux pinning in HTSC materials and a translation of this understanding into manufacturing processes.

We will continue to develop the continuous fiber melt-texturing process described in this report with our efforts focused primarily on studying the relationship between processing conditions, microstructure, and J_c. Clearly, a primary concern in this work is a definition of the parameters which limit the rate at which the YBCO crystallization front moves, as this ultimately determines the rate at which a conductor can be produced. We expect that our effort in this area, especially characterization-related tasks, will be substantially enhanced by our pending

subcontract with the Oak Ridge National Laboratory. At the same time, we will attempt to place samples of this melt-textured fiber in the hands of potential users within the DARPA HTSC Initiative. We have begun this process already, having sent samples to the DARPA program at Boeing Aerospace, NIST-Boulder, and Bio-Magnetic Technologies. We will continue these collaborations in the future and will also supply samples to General Electric and NIST-Gaithersburg. In addition, as part of an EPRI-sponsored program to develop HTSC underground power transmission cables, CPS Superconductor will supply 0.5 meter samples of melt textured fiber Underground Systems, Inc. of Armonk, NY for evaluation. This evaluation will include AC current and AC field characterization which would not otherwise be available.

The BiSCCO work will remain focused on the production of rolled ribbon using the CPS Superconductor wire process. While our primary interest in producing 77 K superconductor material has determined our use of the 2223 BiSCCO as the feedstock for this process, fibers/ribbons will be executed from the 2212 material in the coming quarter to serve as a basis for comparison as well as provide us with the potential for producing 20 K-usable material. Our own in-house work will focus on the post-deformation processing of our ribbon. We have submitted samples of our BiSCCO powder to Los Alamos National Laboratory to be used to produce powder-in-tube wire. Samples of this wire, subsequently processed at both Los Alamos and CPS Superconductor, will be used to serve as a performance baseline for ribbons produced using the CPS Superconductor process.

We will continue our work on melt-textured three-dimensional shapes, both tot provide the active elements of our trapped flux motor and to provide sample parts for potential users within the DARPA HTSC Initiative. We have already submitted samples of melt-textured pellets to Boeing Aerospace and have begun discussions with Mechanical Technologies to produce a melt-textured cylinder for their evaluation. Our development efforts in this area will focus, as in the case of melt-textured fibers, on an elucidation of the relationship between composition and processing and microstructure and performance. In the case of melt-textured shapes, our criteria for performance will be both macroscopic transport J_c, around the circumference of a trapped flux motor magnet replica, for example, and flux trapping. This latter parameter will be measured in-house using a newly acquired fluxmeter and sample jig designed at Emerson Electric.

4. FINANCIAL STATUS

As of September 29, 1990, the project had $4,206,942.00 authorized with a total of $4,205,122.44 expended. No additional funds are required to complete the FY90 fiscal year. An additional $1,304,264.56 will be required in FY91 to meet the contract target of $5,509,387.00.